

Review

Collisional Classical Dynamics at the Quantum Scale

Sebastian Otranto 

Instituto de Física del Sur (IFISUR), Departamento de Física, Universidad Nacional del Sur (UNS), CONICET, Av. L. N. Alem 1253, Bahía Blanca B8000CPB, Argentina; sotranto@uns.edu.ar

Abstract: During the past five decades, classical dynamics have been systematically used to gain insight on collision processes between charged particles and photons with atomic and molecular targets. These methods have proved to be efficient for systems in which numerical intensive quantum mechanical methods are not yet tractable. During the years, reaction cross sections for charge exchange and ionization have been scrutinized at the total and differential levels, leading to a clear understanding of the benefits and limitations inherent in a classical description. In this work, we present a review of the classical trajectory Monte Carlo method, its current status and the perspectives that can be envisaged for the near future.

Keywords: classical trajectory Monte Carlo; cross sections; ionization; charge exchange

1. Introduction

The use of the classical trajectory concept to describe a quantum mechanical process saw its origin in 1936 with the work of Hirschfelder [1]. In this work, a single vibrational trajectory was computed to highlight the potential surface in $H + H_2$ reactions and gain perspective in order to estimate reaction rates for H_3^+ production. With the development of the Monte Carlo method, further efforts were devoted in this direction for the same collision system [2–5]. The first steps in the application of this method, hereafter referred to as classical trajectory Monte Carlo (CTMC), to the ion–atom context were given by Abrines and Percival [6,7]. In their work, electron capture and ionization processes in $H^+ + H$ collisions were explored at the total and singly differential levels. Due to computational limitations, typical simulations in those days were restricted to a limited number of trajectories on the order of a few hundred to a few thousand. The work of Olson and Salop [8] on charge transfer and ionization cross sections by fully and partially stripped positive ions colliding on hydrogen turned decisive gives clear insight on the potentiality of the CTMC method. Since then, and for nearly five decades, CTMC has been routinely used to benchmark novel experimental data and provide theoretical support in fields such as plasma diagnostics and astrophysics.

In this work, we describe the methodology, starting from its early conception, and go through the different adaptations and generalizations that were introduced in the past five decades according to the different contexts of implementation. Following the introduction of the three-body CTMC, emphasis is put on the multielectronic treatment of atoms and molecules. Atomic units are used unless otherwise stated.

2. Materials and Methods

2.1. Classical Trajectory Monte Carlo Method

In its early days, the CTMC model was used to describe collisions involving hydrogenic targets. In this treatment, Hamilton's equations of motion for a mutually interacting three-body system are numerically solved by means of a fourth-order Runge–Kutta method with an adaptive step size.



Citation: Otranto, S. Collisional Classical Dynamics at the Quantum Scale. *Atoms* **2023**, *11*, 144. <https://doi.org/10.3390/atoms11110144>

Academic Editors: Jean-Christophe Pain and Sabyasachi Kar

Received: 30 September 2023

Revised: 5 November 2023

Accepted: 7 November 2023

Published: 9 November 2023



Copyright: © 2023 by the author. Licensee MDPI, Basel, Switzerland. This article is an open access article distributed under the terms and conditions of the Creative Commons Attribution (CC BY) license (<https://creativecommons.org/licenses/by/4.0/>).

$$\begin{aligned}\frac{\partial q_i}{\partial t} &= \frac{\partial H}{\partial p_i}, \\ \frac{\partial p_i}{\partial t} &= -\frac{\partial H}{\partial q_i}\end{aligned}$$

The Hamiltonian for this system reads

$$H = \frac{p_1^2}{2m_1} + \frac{p_2^2}{2m_2} + \frac{p_3^2}{2m_3} + V(r_{12}) + V(r_{13}) + V(r_{23}), \tag{1}$$

where the 1, 2 and 3 subscripts stand for the projectile, electron and nuclear target, respectively. The interaction between particle i and particle j was originally described by means of Coulomb potentials. This one-active-electron formalism was used to describe collisions on atomic targets beyond hydrogen, such as He, Ne and Ar, by introducing effective target nuclear charges in the independent particle model probabilistic scheme [9]. In the following years, more appropriate functional forms for the potential were considered to account for the screening of the nuclear ion by the remaining core electrons [10,11]. In its simplest representation, the active electron–target core interaction can be represented by the sum of a Coulomb potential and a Yukawa potential,

$$V(r_{eT}) = -\left(\frac{Z_{as}}{r_{eT}} + \frac{Z_N - Z_{as}}{r_{eT}} e^{-\lambda r_{eT}}\right). \tag{2}$$

This is equivalent to stating that the electron feels a coordinate-dependent core charge that transitions from the asymptotic charge Z_{as} (equal to 1 for neutral targets) to the nuclear charge Z_N as $r_{eT} \rightarrow 0$. Similar functional forms have been used throughout the years [10–12]. In particular, the parametrization provided by Garvey [13], which also describes a coordinate effective charge and is based on Hartree–Fock calculations, has been extensively used in the ion–atom context. Debye–Hückel or pure Yukawa potentials of the form $Z_a \exp(-r/r_D)/r$ have been used to study collisions of particles with atomic targets embedded in weakly coupled plasmas, either for ion impact [14,15] or electron/positron impact studies [16], while interactions in dense quantum plasmas have been studied by means of a potential of the form $Z_a \cos(r/r_D) \exp(-r/r_D)/r$ [17].

Due to its inherent importance from a basic science perspective, together with its relevance for astrophysical as well as plasma physics environments, hydrogen has been a target of special interest. The CTMC method in its microcanonical description leads to an electron momentum distribution in perfect agreement with its quantum mechanical counterpart. However, it fails to describe the radial distribution, especially at large distances, in which the classical return point provides a sharp limit in contrast to the exponential decreasing behavior exhibited by the quantum mechanical description. During the 1980s, improved descriptions of the CTMC method were designed in order to correct this behavior and study the impact of such modifications at the cross-section level. Eichenaur et al. used the Wigner function for the initial distribution of the coordinates and momenta of the electron instead of the microcanonical phase-space distribution [18]. Hardie and Olson fitted the quantum mechanical radial distribution for ground-state hydrogen by means of a linear combination of microcanonical distributions corresponding to different ionization potentials [19]. These methodologies improved the description of the electron radial distribution, while still providing electron momentum distributions in acceptable accord with the quantum mechanical predictions. In general terms, we hereafter refer to these models as E-CTMC models, noting that they all lead in principle to the same results. Ample use of these strategies has been made in the last few decades [20–22]. During the last decade, Cariatore et al. introduced an alternative model, termed Z-CTMC, in which the radial distribution for H(1s) was fitted by means of a linear combination of microcanonical distributions corresponding to different projectile charges, leaving the ionization potential of the target untouched [21,23]. Differences among the E-CTMC and Z-CTMC models are currently being evaluated in our group for high projectile charges but are expected to

emerge in processes and collision systems that are particularly sensitive to the ionization potential value. In Tables 1 and 2, we include the coefficients and expansion parameters, either ionization potentials or target charge states, for the description of the ground state of the hydrogen atom.

Table 1. E-CTMC binding energies and α_i expansion coefficients for H(1s) [19].

U_i (a.u.)	α_i
2	0.016
1	0.0984
0.6667	0.1923
0.5	0.2185
0.4	0.1849
0.3333	0.1349
0.2857	0.0920
0.25	0.0630

Table 2. Z-CTMC nuclear charges and α_i expansion coefficients for H(1s) [21].

Z_i	α_i
0.5	0.0724
0.625	0.07658
0.75	0.09665
0.875	0.09230
1.0	0.16204
1.25	0.17971
1.5	0.13019
1.75	0.08071
2.0	0.06475
2.5	0.04493

In the next section, we compare the behavior of the Z-CTMC, the E-CTMC and the CTMC models for electron capture processes.

2.2. Electron Capture

The study of electron capture processes following ion impact dates back to the 1920s, when our understanding of the atom was migrating from Bohr’s model to the framework of the novel quantum theory [24–26]. In 1954, Bohr and Lindhard introduced a classical model to estimate the total cross section [27]. By assuming that the single capture (SC) of the target electron would take place whenever the force exerted by the projectile of charge Z_P on the electron exceeds that of the target nucleus, they were able to determine a reaction boundary impact parameter b_{max} that leads from H(1s) to a geometrical cross section $\sigma_{SC} = \pi b_{max}^2 = Z_P(4 - 10) \times 10^{-16} \text{ cm}^2$. We note the absence of any energy dependence and that this result predicts a linear dependence on the incident ion charge. Since all the electron flux was assumed to go to the single-electron capture process, this theory is valid only at low collision energies. At high impact energies, two additional issues must be considered. On the one hand, capture does not occur unless the electron acquires the necessary kinetic energy to leave the reaction with the projectile. This situation establishes a capture radius R_{cap} . On the other hand, the geometrical cross section πR_{cap}^2 now contains information on the whole electron loss channel. The information on the capture channel is then extracted by multiplying the geometrical cross section by the capture probability given by the ratio of the collision time to the orbital period of the target electron. The obtained high energy limit for the capture cross section is then given by $\sigma_{SC} = 8\pi Z_P^3 / (n_i^3 Z_T^5 E^{7/2})$.

Following a similar line of reasoning, during the 1980s, the classical overbarrier model (COB) was introduced [28–31]. In this model, the electron energy and the height of the potential barrier generated by both projectile and target ion core potential wells are tracked

as the projectile approaches the collision region. Once the projectile reaches the critical internuclear distance R_c , at which the electron energy equals the top of the barrier, the electron can escape from the target potential well and get captured by the projectile. In this case, the total capture cross section is given by $\sigma_{SC} = 8\pi R_c^2$. As in the Bohr and Lindhard model, this geometrical cross section should be multiplied by the capture probability, since the crossing of the barrier by the electron can either lead to capture or ionization. One clear advantage of the COB is that it allows to determine the n -state at which the electron is most expected to be captured, although no information is provided on the n -distribution as long as resonant capture is assumed. The introduction of a reaction window in the extended overbarrier model, consisting in a Gaussian distribution of binding energies centered in the value corresponding to the most probable value, allows inferring the n -distribution [29,31]. Regarding the l -distributions, Burdgorfer et al. proposed a simple extension of the COB model to predict the average angular momentum of an electron captured to high n -values for slow highly charged projectiles [32]. In their model, the electron's angular momentum in the projectile frame is assumed to be conserved during the electron capture process. This simple qualitative approach led to reasonable agreement with the reported (n,l) -state selective cross sections for collisions involving O^{6+} and N^{5+} projectiles on $H(1s)$ and H_2 targets in the impact energy range 1–6.25 keV/u.

The CTMC predictions are in agreement with the absence of energy dependence in the low-energy range, while it naturally leads to the $E^{-7/2}$ dependence at large impact energies, in concordance with the outcomes of the Bohr and Lindhard model [33,34]. In Figure 1, we show the CTMC total cross section for single-electron capture as a function of the projectile charge Z_p .

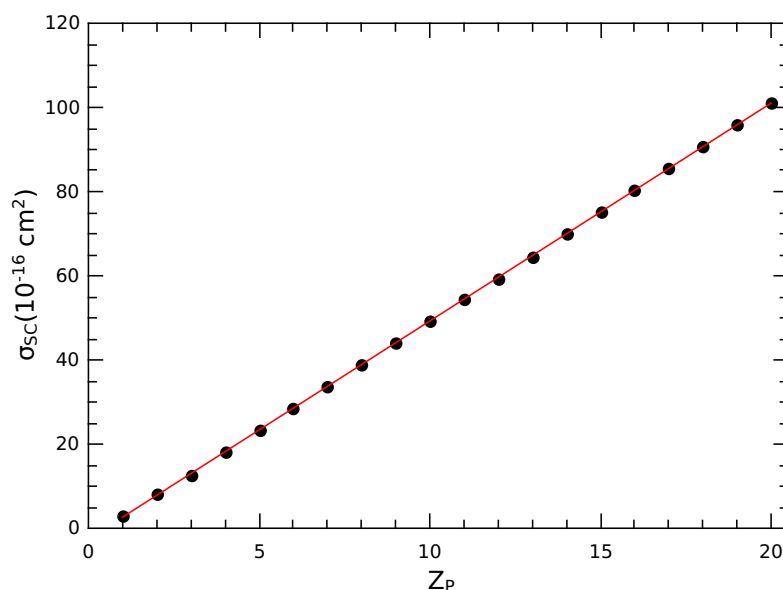


Figure 1. CTMC total cross section for single electron capture (SC) from H as a function of the projectile charge Z_p at an impact energy of 25 keV/u. A linear fit is incorporated in red to highlight the strict linear dependence on Z_p .

A major step forward in our understanding of the charge exchange process from a classical perspective was achieved with the article published by Olson in 1981 [35]. In this work, the (n, l) -state-selective electron capture cross sections following the collision of projectiles of positive charge Z_p with $H(1s)$ were studied by means of the CTMC model. For each trajectory corresponding to electron capture, the binding energy E_p of the electron relative to the projectile was determined and related to a classical value n_c by using

$$E_p = -\frac{Z_p^2}{2n_c^2}. \tag{3}$$

The n_c values were finally binned into discrete n -values by the condition of Becker and McKellar [36]:

$$[(n - 1)(n - 1/2)n]^{1/3} \leq n_c \leq [(n + 1)(n + 1/2)n]^{1/3}. \tag{4}$$

Regarding the n -distribution, it is worth discussing the expected behavior according to the physical properties of the collision system. If one assumes that during the electron capture process the electron preserves its orbital energy, then

$$E = -\frac{Z_T^2}{2n_i^2} = -\frac{Z_P^2}{2n_f^2}, \tag{5}$$

leading to $n_f = n_i Z_P / Z_T$. On the other hand, if the dimension of the electron orbit is the expected quantity to be preserved during the electron capture process, we obtain

$$\langle r \rangle = \frac{n_i^2}{Z_T} = \frac{n_f^2}{Z_P}, \tag{6}$$

leading to $n_f = n_i (Z_P / Z_T)^{1/2}$.

CTMC calculations show that the n -state-selective cross sections maximize at $n_f = n_i Z_P^{3/4}$, exhibiting a compromising behavior between these two limits. In Figure 2, we illustrate this trend for the $O^{8+} + H(1s)$ collision system and highlight, as the impact energy increases, how the n -distribution attains the n^{-3} scaling already predicted by Oppenheimer in 1928.

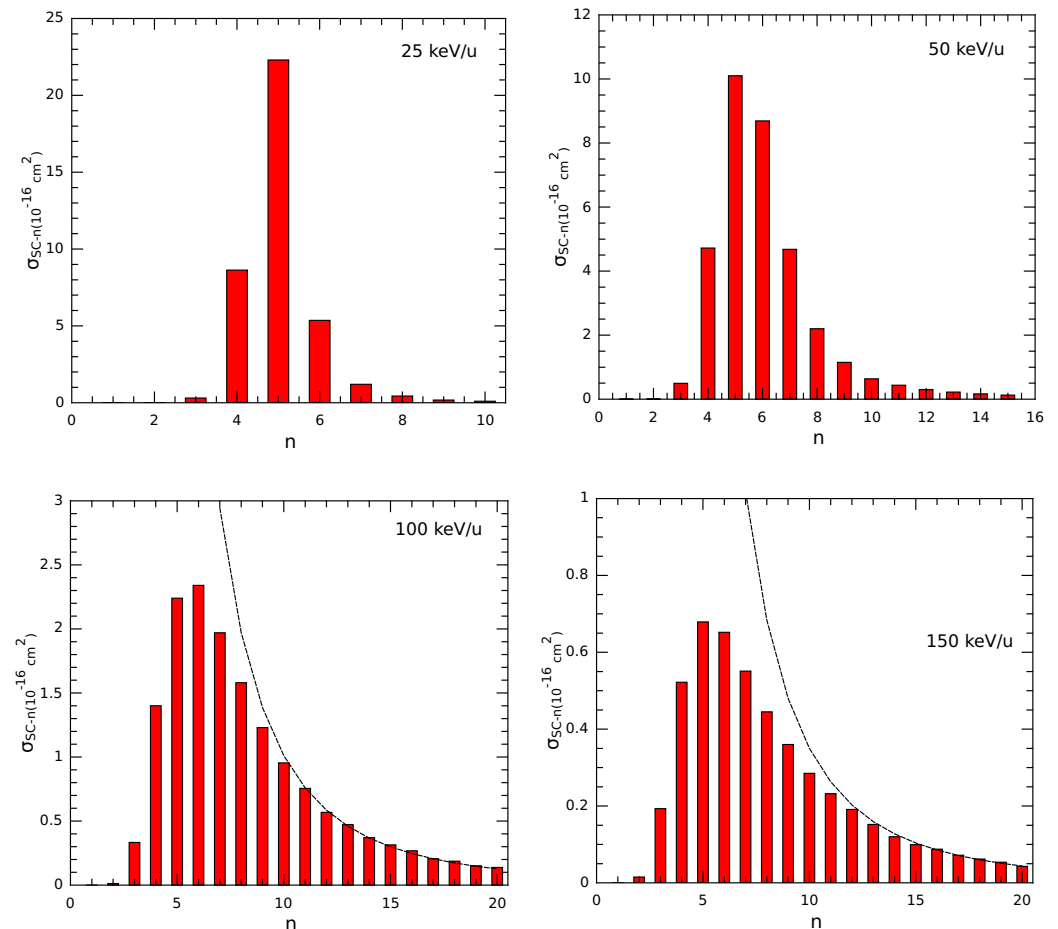


Figure 2. CTMC n -state-selective charge-exchange cross sections for $O^{8+} + H(1s)$ collisions. The dashed line indicates the n^{-3} scaling expected for the population of high n -values.

Now, and in contrast to the Bohr–Lindhart and COB models, the CTMC method inherently provides information on the l -distribution of the electron captured to a given n -value. The l -values are similarly obtained from the normalized classical angular momentum $l_c = (n/n_c)(\mathbf{r} \times \mathbf{k})$ by means of the binning procedure, with \mathbf{r} and \mathbf{k} being the position and momentum of the captured electron relative to the projectile

$$l \leq l_c < l + 1. \quad (7)$$

It is worth noting that the l -distributions depend on the collision energy. Low l -values are populated at low-impact energy collisions, while a statistical population is approximated as the impact energy is increased. The CTMC method naturally merges these two limits without the need of invoking any ad hoc assumptions. This feature is illustrated in Figure 3, where the $(n = 5, l)$ -state-selective capture cross sections are displayed for $\text{O}^{8+} + \text{H}(1s)$ collisions at impact energies in the range 25–500 keV/u. For each impact energy considered, a dashed line that reflects a statistical distribution arbitrarily normalized to the $(5, 2)$ cross section is also included. For impact energies in the range 25–150 keV/u, we observe that the population of the larger l -values is overstatistical. This behavior has been analyzed by Olson for projectile charges $Z_p = 2$ –20 and was found to be typical of electron capture to n -values lower than the n_{max} at which the distribution maximizes [35]. It should be noted though that if the energy is pushed to even larger impact energies, entering a domain in which the ionization channel becomes dominant, the population reverts to low l -values. This obeys to the fact that velocity matching between the projectile and the target electron is the route by which electron capture proceeds. This is consistent with highly eccentric orbits associated to low l -values.

In Figure 4, we present the n -state-selective electron capture cross section for C^{6+} and O^{8+} collisions on $\text{H}(1s)$ at an impact energy of 10 keV/u. The classical results predicted by the Z-CTMC, E-CTMC and CTMC methods are compared with the Atomic Orbital Close Coupling (AOCC) calculations performed by the group of Aumayr [37,38]. As a general trend, we first notice that the Z-CTMC, CTMC and AOCC methods agree on the n_{max} -value at which the distribution attains its maximum. The E-CTMC distribution, in contrast, predicts a larger n_{max} -value. Second, the CTMC method clearly underestimates the electron capture to levels with $n > n_{\text{max}}$. This behavior tends to be corrected by both the Z-CTMC and E-CTMC methods due to their improved description of the $\text{H}(1s)$ radial distribution. Overall, the E-CTMC provides the widest distribution, while the Z-CTMC distribution seems to be the one in closer agreement with the AOCC method, specially for the O^{8+} case.

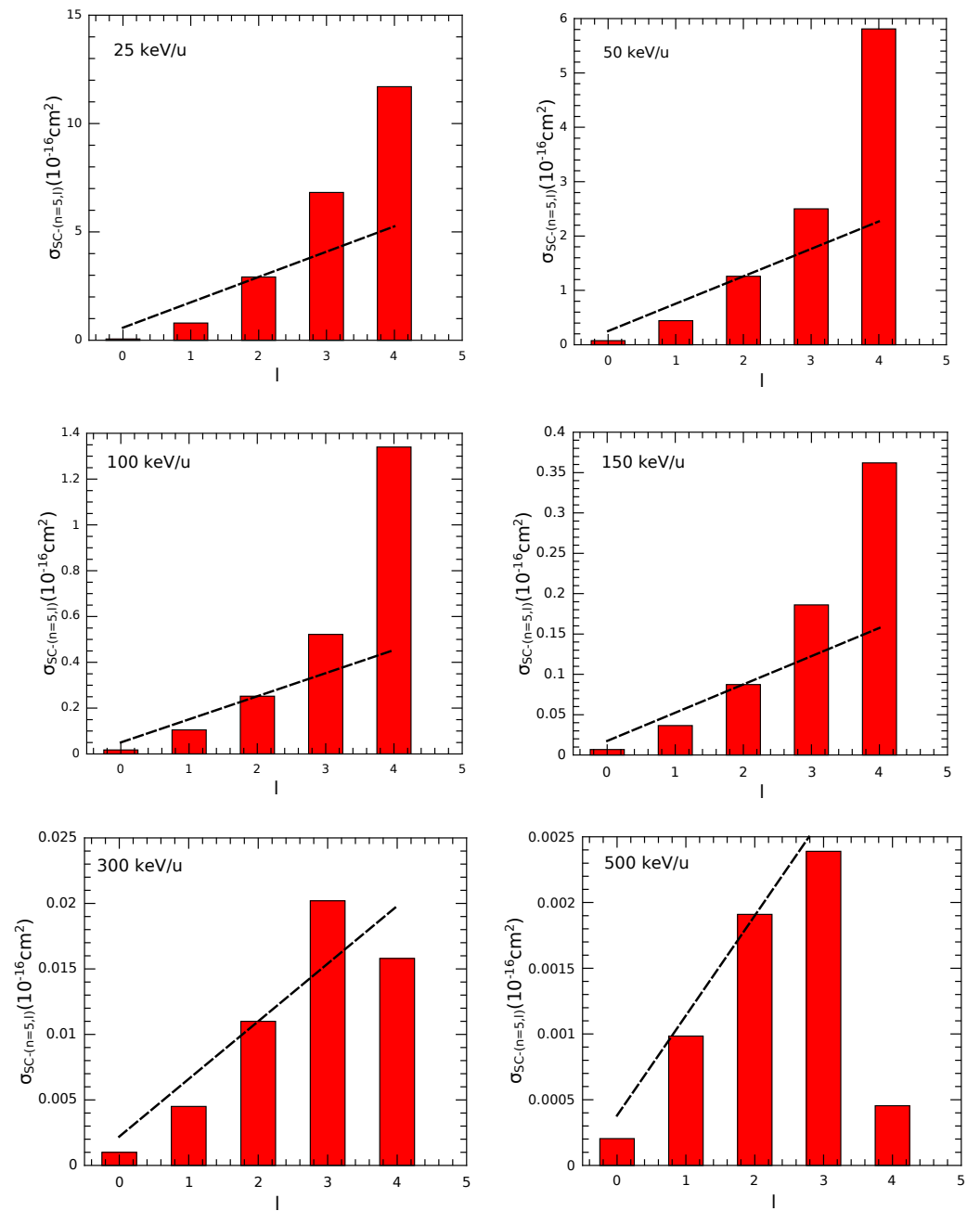


Figure 3. CTMC (5,l)-state-selective charge-exchange cross sections for $O^{8+} + H(1s)$ collisions: The dashed line indicates a statistical distribution arbitrarily normalized to the (5,2) cross section.

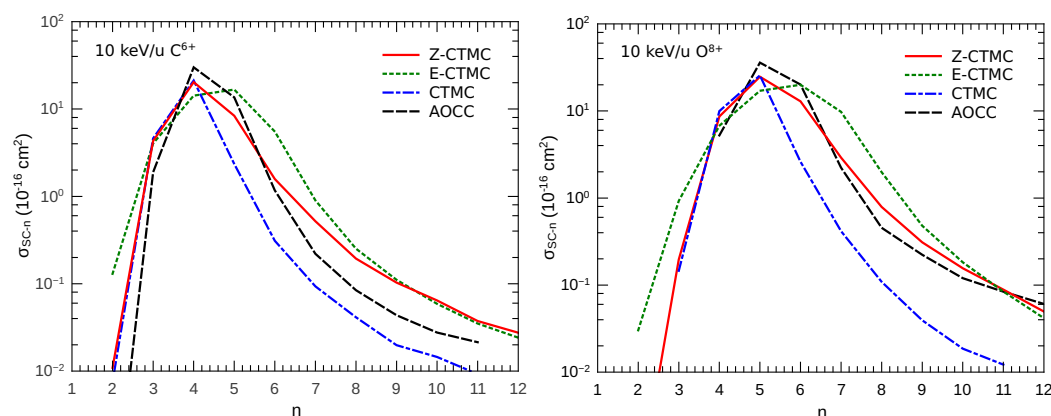


Figure 4. Theoretical n -state-selective charge-exchange cross sections C^{6+} and O^{8+} collisions on $H(1s)$ at 10 keV/u. The Z-CTMC, E-CTMC and CTMC results are contrasted with those obtained by Igenbergs et al. by means of the AOCC method [37,38].

2.3. Ionization

Electron emissions originating in collisions involving charged particles and neutral targets has been a challenging field since the 1920s. Particular interest in ionization processes developed in the field of astronomy, specifically for the characterization of stellar atmospheres [39]. With the development of quantum mechanics, early studies by Bethe based on the First Born Approximation (FBA) analyzed electron emission by charged particle impact [40]. In spite of the interest in ionization processes, our improvement in our understanding of the field had to wait until the development of sophisticated vacuum techniques in the 1960s that allowed measuring low-energy electrons with confidence [41–46]. These pioneering experiments opened the door to subsequent studies that up to the present day keep shedding light on many features in electronic distributions and challenge their interpretation in terms of collisionistic mechanisms.

From a theoretical point of view, the availability of electron emission differential data soon revealed that the FBA was far from providing the ultimate word and that signatures of the denominated two-center problem, i.e., fingerprints in the electronic distributions due to the joint influence of the target ion and the projectile in the emitted electron dynamics, were not properly accounted for in such one-center models. For positive ion impact, the most clearly visible trend was an enhancement of the electron forward emission, including an asymmetric cusp-shaped peak that highlights the electron capture to the projectile continuum (ECC) [47]. This peak that was theoretically reproduced by distorted wave models that considered, in the final channel, the interaction of the emitted electron with both target ion and projectile, even through a separable wavefunction consisting of the product of two separate distorted waves, one for each interaction [48]. This was the case of the Born-3C [49] and the continuum distorted wave–eikonal initial state (CDW-EIS) [50–53].

Classical studies within the CTMC method have proven to be particularly efficient in describing the ECC peak structure in ion–atom collisions. Studies by Reinhold and Olson regarding the ECC peak formation in $H^+ + He$ and $He^{2+} + He$ collisions showed that the dynamical formation of the ECC peak is mediated by two mechanisms: (i) the focusing of emitted electrons due to interaction with the projectile and (ii) electron capture to highly excited states of the projectile that could undergo a transition to the continuum due to the influence of the residual target, even at large internuclear distances [54]. In both cases, electron trajectories must be tracked up to very large internuclear distances to achieve convergence and delineate the peak structure. Trajectories that are ended before reaching their asymptotic velocities leave clear traces in the predicted spectrum, leading to a hole with no events in the peak region. Therefore, by ending the trajectories at different internuclear values, they were able to highlight how the ECC asymmetry is built. The infinite separation limit was obtained by analytically extending the integration of the trajectories from some point onward. Barrachina and Courbin later showed for $H^+ +$

H(1s) collisions that the analytical extension of the electron trajectories can be started, even at short internuclear distances, once the mechanism (i) turns dominant [55]. Further studies include the analysis of the ECC structure for $H^+ + H$ and $H + H$ collisions [56] and $H^+ + He$ collisions [57], as well as in the context of transfer ionization studies involving Ar targets [58]. In order to illustrate this issue, in Figure 5, we show the electron emission in momentum space for 100 keV $H^+ + H(1s)$ collisions. Simulations were stopped once the projectile reached a distance r_{stop} , with respect to the laboratory frame, located on the center of mass of the initial target system. It can be observed that the hole-like structure described in the works of Reinhold et al. and Barrachina and Courbin for the ECC peak clearly shows up in this representation at $(k_{e-par} = 2, k_{e-perp} = 0)$, and it tends to narrow as the r_{stop} -value is increased. Moreover, the same situation is clearly identified in the region at $(k_{e-par} = 0, k_{e-perp} = 0)$. However, it should be noted that a proper description of this region requires a quantum mechanical description, since the production of low-energy electrons originates in soft collisions and is governed by dipole-like transitions, which are not included in the classical model.

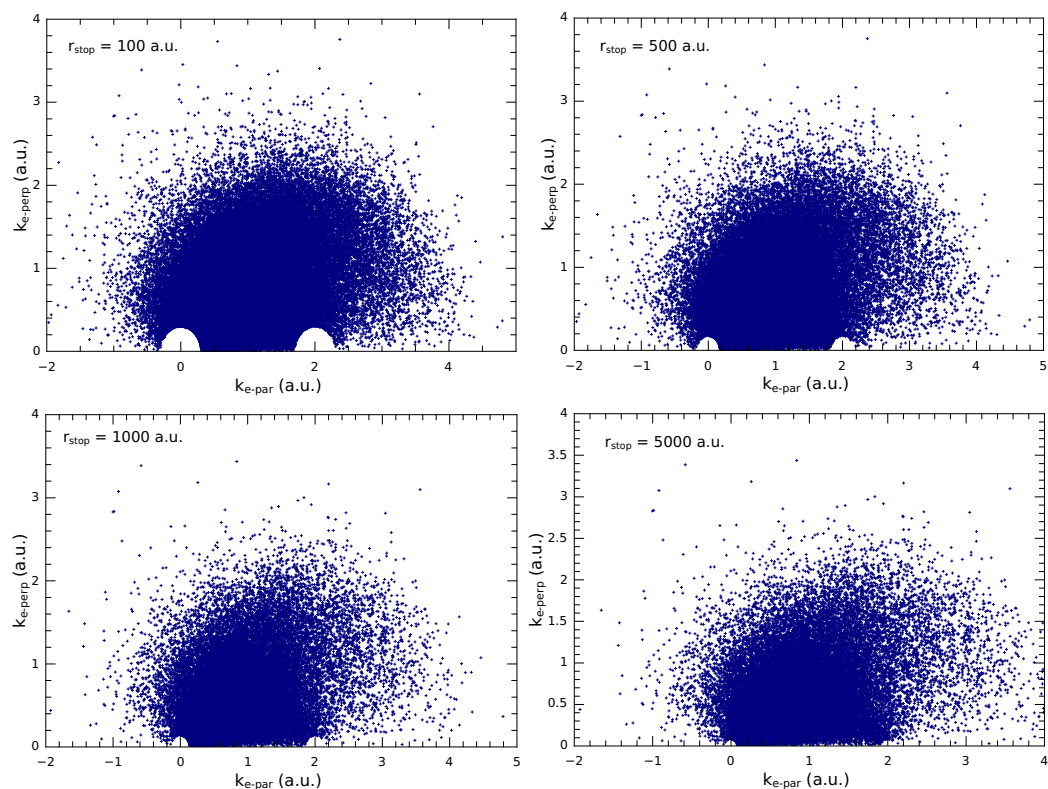


Figure 5. CTMC electron emission events represented in momentum space for 100 keV $H^+ + H(1s)$ collisions.

During the 1990s, the development of the Cold Target Recoil Ion Momentum Spectroscopy (COLTRIMS) technique gave access to the denominated kinematically complete experiments. By detecting the recoil ion in coincidence with the emitted electron, and by recalling the energy conservation and the momentum conservation equations for the whole system, the momenta of all the fragments involved in a given collision process were identified (see [59] for a review). The COLTRIMS technique introduced a change in perspective in the way in which collisional data are analyzed. For instance, single-differential cross sections, in terms of the longitudinal momentum of the recoil ion, provided new ways to analyze the previously explored structures, such as the ECC peak or the soft electron peak [60,61]. Being a computational simulation of the experimental procedure, the CTMC method naturally adapted to these new representations and provided theoretical support in the early years for this novel technique [62,63].

Now, moving to ionization processes due to light-particle impact, the advances achieved in electron coincidence techniques by the end of the 1960s allowed measuring triply differential ionization cross sections by electron impact [64,65]. By 2003, a reaction microscope based on the COLTRIMS technique was operational [66]. The measurement of fully differential cross sections for positron impact within the COLTRIMS technique would follow soon after [67,68]. Just as in the ion-impact case, the FBA soon showed its limitations, and more sophisticated distorted-wave models were developed, like the Distorted-Wave Born Approximation (DWBA) [69]; the Born-3C model, including its subsequent variants [70–72]; the CDW-EIS [73–76]; the introduction of highly intensive numerical methods such as Time-Dependent Close Coupling (TDCC) [77]; Convergent Close Coupling (CCC) [78]; and the B-spline R-Matrix approach [79], among others. From the CTMC perspective, a comparison of single-electron removal processes in the collisions of electrons, positrons, protons and antiprotons with H and He at the total cross-section level was published by Schultz by the end of the 1980s [80]. This work was followed soon after by differential analyses in positron collisions with He, Kr and H₂ [81,82]. Positron studies at the differential level were also carried out within the CTMC method by groups at Bariloche [83–85], Debrecen [86] and Bahía Blanca [16]. These studies, provided further insight on the physical mechanisms mediating the ECC peak structure, as well as the dynamical orientation of the positron-emitted electron pair in the continuum. A recent study on electron–carbon collisions has shown that the CTMC method can provide a good description of the total cross section from the threshold up to at least 1 keV, in agreement with theories such as Time-Dependent Close Coupling, R-matrix with pseudostates and the B-spline R-matrix with pseudostates [87]. Despite the large set of fully differential cross sections reported for the ionization of hydrogen and noble gases by electron impact, comparisons at this level between the CTMC and the quantum mechanical models above described are scarce and, to our knowledge, amount to those performed by Geyer and Rost, cited below in Section 2.5.6.

Regarding multiple photon impact ionization, during the past two decades, the COLTRIMS technique has been combined with intense few-cycle pulses, thus allowing the detailed study of the physical mechanisms leading to multiple-electron removal [88–94]. Emphasis has been placed on determining the mechanisms of Sequential Double Ionization (SDI) and Nonsequential Double Ionization (NSDI). While SDI considers that electrons are independently emitted by the laser field, the NSDI mechanism implies a temporal sequence in which the double ionization is mediated by the electron–electron correlation. The nonsequential mechanism is not restricted to double ionization and can be extended to higher-order ionization [95]. These mechanisms were identified back in 1990, after noticing that theoretical SDI models in a one-active-electron description were able to reproduce the experimental data for field intensities greater than 4×10^{-15} W/cm² but could not reproduce the electronic production detected for lower field intensities [96]. Below $\times 10^{-15}$ W/cm², multiple-electron emission exceeded by six orders of magnitude the predictions of the SDI. In the last few years, studies have also been extended to the nondipolar case by explicitly including the magnetic field. This field has been shown to play an important role in the NSDI for Ne and Xe targets [97,98].

From a theoretical point of view, quantum and classical models alike have been used. Among the former, we can cite the numerical solution of the time-dependent Schrödinger equation [94,99,100], models framed within the strong field approximation [101] and the multiple scattering quantitative theory [102]. The CTMC model was, to our knowledge, first implemented in this context by Cohen [103], who studied the ionization of the hydrogen ion in an intense laser field and compared the classical results with those predicted by the numerical solution of the time-dependent Schrödinger equation. In this work, a dynamical incorporation of tunneling at the classical turning points was performed.

In the following sections, we detail the specific models that have been proposed and used throughout the years to treat multielectronic targets in the different fields described above.

2.4. Multiple-Electron Targets via One-Active-Electron Models

Multielectronic atomic targets were initially considered in the framework of the three-body CTMC method by means of the independent electron model (IEM) [104]. This model assumes a collision period sufficiently brief enough that the electrons cannot rearrange themselves during the collision. By neglecting correlation effects, the multiple-electron transition probabilities $P_n(b)$ associated to the removal of n electrons from a shell containing N electrons at a given impact parameter b is modeled as follows:

$$P_n(b) = \binom{N}{n} P_s(b)^n (1 - P_s(b))^{N-n}, \quad (8)$$

where $P_s(b)$ refers to either the single-ionization or the single-electron capture probabilities, which are, respectively, denoted as $P_{SI}(b)$ and $P_{SC}(b)$. By the end of the 1970s, this model was used to obtain single-electron capture and single-ionization cross sections for multiply charged ion collisions on He [105]. The multiple ionization of He, Ne and Ar by highly stripped projectiles was also studied by the same group at that time [9]. This methodology was also used to describe the dynamics of antimatter–atom collisions, considering proton, antiproton, electron and positron collisions on He, and predicted large global effects in the ejected-electron spectra for ionizing collisions when the mass and the charge sign of the projectile are varied [106]. Alternatively, the Independent Events Model (IEV) [107], in which the full rearrangement of the target ion is assumed following the removal of a first electron has also been employed [12,108,109]. One-active-electron treatments have also been used to deal with alkali metals, such as Li(2s), Na(3s) and Na*(3p). In these cases, Garvey-type potentials have been employed to represent the target ionic core. This model has reasonably predicted the line emission cross sections for C⁶⁺ and O⁸⁺ + Li(2s) collisions [110] and He²⁺ + Na(3s) collisions [111]. Furthermore, the initialization of the electron orbits restricted to the different planes relative to the projectile's incident velocity allowed determining state-selective electron capture cross sections and line emission cross sections on oriented Na*(3p) targets and analyzing their impact velocity dependence [112,113]. More recently, this methodology successfully reproduced the longitudinal and transverse recoil ion momentum distributions measured at KVI by means of their magneto–optical trap recoil ion momentum spectroscopy (MOTRIMS) device [114]. Moreover, an oscillatory structure detected at low-impact energies in the experimental transverse recoil ion distributions has been correctly reproduced with this model and ascribed to electron oscillations around the potential saddle position [115–117]. Moving to the molecular case, pure one-active-electron treatments have been used within the Coulombic approximation to deal with targets for astrophysical purposes. Specifically, CTMC cross sections obtained under such approximation successfully reproduced the X-ray spectra for comets C/Linear 1999 S4 and McNaught–Hartley C/1999 T1, detected by the Chandra X-ray observatory [118,119], and allowed estimating the sensitivity of the spectra to the solar wind ionic fluctuations during the detection period. A similar model was used by Borbély et al. to describe the ionization of H₂O by intense ultrashort half-cycle electric pulses [120]. The classical results were found to be in agreement with the quantum mechanical predictions at high intensities, where the over-the-barrier ionization mechanism is dominant compared with tunneling ionization, which is not included in their CTMC model.

2.5. Explicit Multiple-Electron Descriptions of He

It is well known that atoms beyond hydrogen cannot be fully treated in classical terms, since the interelectronic correlation leads to their autoionization. Therefore, different strategies have been proposed during the past four decades with the aim of incorporating the electron–electron correlation or their dynamical screening effects. Due to its relevance from a basic science perspective, helium is a target on which much focus has been put in the last decades in order to gain insight into the role of the interelectronic correlation effects in different collisions processes. In what follows, we describe different strategies that have

been proposed in the past four decades to explicitly model this two-electron atom. We refer to H_0 as the physical Hamiltonian for He,

$$H_0 = \frac{p_1^2}{2} + \frac{p_2^2}{2} - \frac{Z_T}{r_1} - \frac{Z_T}{r_2} + \frac{1}{r_{12}}, \quad (9)$$

2.5.1. The Heisenberg Core CTMC

In 1980, Kirschbaum and Wilets introduced restoring potentials to the Hamiltonian of multielectronic atoms in order to fulfill the Heisenberg uncertainty principle and the Pauli exclusion principle upon a classical atom [121]. These additional potential terms for the full two-electron Hamiltonian read

$$H = H_0 + V_{HC}(r_1, p_1) + V_{HC}(r_2, p_2), \quad (10)$$

with

$$V(r_i, p_i) = \left(\frac{\zeta^2}{4\alpha r_i^2} \right) \exp \left\{ \alpha \left[1 - \left(\frac{r_i p_i}{\zeta} \right)^4 \right] \right\}. \quad (11)$$

Here, α is called the hardness parameter and ζ is related to the size of the core. For r_i and p_i values, such that $r_i p_i \leq \zeta$, this potential becomes strongly repulsive, and the electrons cannot get close to the nucleus, thus avoiding its autoionization.

By using this model, hereafter denominated HC-CTMC, Zajfman and Maor obtained total charge exchange and ionization cross sections for proton impact which were in better agreement with the experimental data at impact energies greater than 50 keV and 100 keV, respectively [122]. This model was later revisited by Cohen [123], who showed that the total cross sections for single capture and ionization are more sensitive to variations in ζ rather than α . In this work, and for each α -value analyzed, he proposed a ζ -value in order to match the first ionization potential of the target. Morita et al. studied the minimum ζ -value for a fixed α -value that would avoid autoionization [124]. A decade ago, Zhou provided a different criterion to determine ζ in the laser-argon sequential double-ionization context. They determined the ζ parameter by requiring the one-electron Hamiltonian to minimize at the second ionization potential of the two-electron atom [125]. They showed that compared with the independent-electron model, this correlated description led to an improved quantitative agreement with the available data for the ion momentum distributions and the measured ionization time for the second electron. A more punctual analysis of the implications of ζ for the He target electronic distribution was recently performed by Bachi and Otranto [126,127]. It was found that a ζ -value under the criterion of Morita et al. leads to a target dynamic in which one electron is close to the nucleus while the other is distant. In contrast, a ζ -value under the criterion of Zhou et al. leads to a Bohr-like atom, with both electrons situated at similar distances from the nucleus and opposite each other in order to maximize the shielding. As a point aside, we note that very recently, the group of Tokesi performed an intensive study of the proton + H(1s) system with the correction term proposed in this model. The aim, in this case, was that of incorporating the Heisenberg correction term [128,129]. In their study, they showed that compared with the CTMC model, the introduction of the correction term improved the agreement in the charge-exchange channel, while it turned out to not be relevant for the ionization channel.

2.5.2. The Bohr Atom

For He atoms, the Bohr picture (two electrons rotating in circular orbits opposite to the nucleus, thus defining an orbital plane) was employed by the Olson's group [130–132]. At the total net ionization cross-section level, this treatment corrected a systematic trend of the IEM model: the underestimation (overestimation) of the single (double)-electron removal cross sections. Moreover, the enhanced double-ionization cross sections of He for antiproton impact relative to proton impact was properly reproduced. Nevertheless, at low-impact energies, autoionization events can still become an issue if the impinging

projectile field affects the Bohr atom geometry before reaching the reaction region, thus forcing to start trajectories with the projectile already close to the reaction region.

2.5.3. The Split-Shell Model

In 1986, Olson et al. introduced the split-shell model to study single- and double-electron capture and ionization and transfer ionization processes for incident ion charges +1 to +50 at an impact energy of 1 MeV/u [133]. In this model, the electrons are sorted with sequential binding energies and their corresponding effective charges $Z_{eff,i}$ according to the Coulombic prescription $Z_{eff,i} = \sqrt{2n_i^2|\epsilon_i|}$. The impact energy dependence predicted by this model for the double-electron capture process was evaluated by Tórkési and Hock. In their study, this four-body description of the $\text{He}^{2+} + \text{He}$ collision system was evaluated up to an impact energy of 1500 keV/u. Good agreement was found with the reported data and with other theoretical approaches [134].

2.5.4. The Dynamical Screening CTMC

This model was introduced by Montemayor and Schiwietz in 1989 and is referred to hereafter as dCTMC [135]. The idea in this case was to incorporate radial correlation among the electrons, which amounts to taking into account the electron screening effect without any information on the relative distance among them. To do so, they assumed the electronic density of each electron to be given by the 1s hydrogenic wavefunction, with an effective charge $\zeta = 1.6875$ and an ionization energy $I_{1s} = 0.89648$ a.u. By using Gauss's law, the electric potential generated by the nucleus and one of the electrons at a given r -value can be easily determined, which allows determining the potential energy term corresponding to each electron. The dCTMC Hamiltonian is then given by

$$H_{dCTMC} = \frac{p_1^2}{2} + \frac{p_2^2}{2} - \frac{Z_T}{r_1} - \frac{Z_T}{r_2} + V_{ee,1}(r_1, \zeta_2) + V_{ee,2}(r_2, \zeta_1), \quad (12)$$

with

$$V_{ee,i}(r_i, \zeta_j) = \frac{1 - (1 + \zeta_j r_i) \exp(-2\zeta_j r_i)}{r_i}, \quad (13)$$

and $j \neq i$. A dynamical, i.e., collisional time-dependent, model for the ζ_j parameter was implemented and is given by

$$\zeta_j(t) = \begin{cases} 0 & \text{for } I_j \leq 0 \\ (\zeta_{1s}/I_{1s})I_j(t) & \text{for } 0 < I_j < I_{1s} \\ \zeta_{1s} & \text{for } I_{1s} \leq I_j \end{cases} \quad (14)$$

The analysis of He single and double ionization by H^+ impact at the total and differential levels showed that the inclusion of radial correlation improved the description compared with simulations based on the independent electrons scheme [135]. Subsequent dCTMC studies performed by Meng et al. focused on the transverse recoil ion distributions in proton/antiproton collisions with He, finding close agreement with the available data [136]. This model has been used to identify the electron capture mechanisms in $\text{He}^+ + \text{He}$ collisions at intermediate- to low-impact energies, leading to good agreement with state-selective charge-exchange cross sections measured by means of the Cold Target Recoil Ion Momentum Spectroscopy (COLTRIMS) technique [137,138]. Much more recently, this method was extended to analyze the double and triple ionization of three-electron atoms driven by intense infrared laser pulses [139].

2.5.5. The Energy-Bounded CTMC

In 1996, Cohen proposed a different strategy to describe the He-atom based on the introduction of an energy constraint potential,

$$H = H_0 + V_{EB}(r_1, p_1) + V_{EB}(r_2, p_2), \quad (15)$$

with

$$V(r_i, p_i) = \frac{Z_T}{r_i} \exp\left(\frac{E_0 - E_i^{Coul}}{\Gamma}\right), \tag{16}$$

and

$$E_i^{Coul} = \frac{p_i^2}{2} - \frac{Z_T}{r_i}. \tag{17}$$

In this case, Γ plays the role of the numerical parameter on which the sensitivity is weaker, while the constant E_0 is determined by matching the minimum of the one-electron Hamiltonian to the second ionization potential of the target [123]. This model, hereafter denominated EB-CTMC, has been used to describe single-electron capture and ionization following H^+ , He^{2+} and Li^{3+} collisions [123], single-electron capture, single and double ionization and transfer ionization in H^+ collisions and single capture and single ionization in C^{6+} and $(O)^{8+}$ collisions [126]. Differential cross sections in terms of the longitudinal and transverse momentum of the collision fragments, and as a function of the electronic geometries during double-ionization processes, have also been studied [127]. In Figure 6, we show an events plot for the interelectronic distance as a function of one of the electron's radial coordinates. In these models, the corresponding parameters are $\alpha = 2.0$, $\xi = 0.894$, $\Gamma = 0.3$, $E_0 = -2.91$ a.u., thus corresponding to the situation in which the second ionization potential is used as the minimum attainable value for any of the electrons. It can be observed that in this configuration, the EB-CTMC provides a much wider spatial range for the evolution of both electrons compared with the HC-CTMC model.

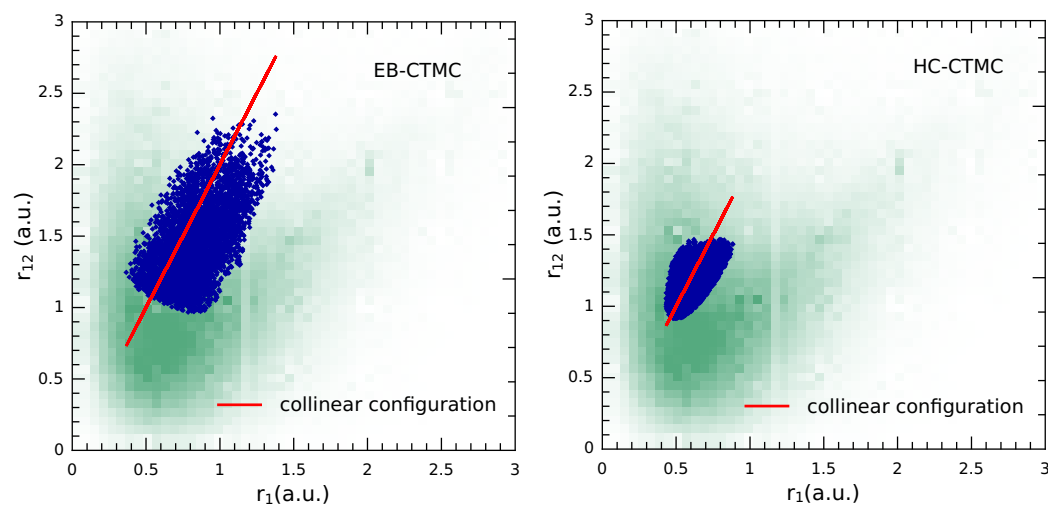


Figure 6. Interelectronic distance as a function of one of the electrons' radial coordinates for the EB-CTMC and HC-CTMC models. The overlapping density plot in green represents the radial 2-particle density predicted by a correlated variational wavefunction.

These classical distributions are compared, using the same representation, with the two-particle radial density $(4\pi)^2 r_1^2 r_2^2 |\Psi(r_1, r_2, r_{12})|^2$ predicted by a variational correlated wavefunction introduced by Bonham and Kohl [140]. In agreement with the classical predictions, the quantum mechanical density exhibits its maximum close to the collinear geometry. However, the electrons are preferably closer to the nucleus and, as expected, the resulting distribution is spatially more extended.

2.5.6. The Quasi-Classical Møller Approach

In this model, the He atom is modeled by means of the exact Hamiltonian H_0 . The projectile–target interaction is initially turned off, and each trajectory is propagated backwards in time until the projectile and target are well separated from one another. Since the He atom is unstable, it autoionizes during this backward propagation stage. At this point, the projectile–target interaction is turned on, and the whole system is propagated

forward in time. As the projectile approaches the target, it initially has a negligible effect on the He target. Meanwhile, the atom focuses and recovers the two-electron bound state. As a result, the projectile is expected to find a correlated two-electron target described by the exact Hamiltonian. By doing so, there is no need to introduce stabilizing potentials or to neglect some part of the electron–electron interaction, such as the angular correlation. Between 2001 and 2004, Geyer and Rost tested and implemented this model to study the single and double ionization of He by electron impact at the total, single-differential and fully differential levels [141–144]. Their results suggest that this strategy provides a good description of the double-ionization total cross section, especially at impact energies lower than those at which the cross section peaks. This region is extremely sensitive to the angular correlation, as suggested by the dCTMC studies of Montemayor and Schiwietz. However, it should be noted that the methodology has not been pushed further, specially for bare ion impact, where the influence of the projectile–target interaction could manifest well before the projectile reaches the target region.

2.5.7. The Soft-Core Coulomb Potential Model

This model was introduced by Haan et al. in 2006 to analyze the strong-field double ionization of He [145,146] based on previous one-dimensional models [147–149].

In this model, the two-electron Hamiltonian reads

$$H_0 = \frac{p_1^2}{2} + \frac{p_2^2}{2} - \frac{Z_T}{\sqrt{r_1^2 + a^2}} - \frac{Z_T}{\sqrt{r_2^2 + a^2}} + \frac{1}{\sqrt{r_{12}^2 + b^2}}, \tag{18}$$

where a and b are empirically determined in order to avoid the autoionization of the atom. Specific values reported by Haan et al. to achieve stability are $a = 0.825$ a.u. and $b = 0.05$ a.u. The authors initialized the electrons by means of radial Gaussian distributions by giving each electron zero angular momentum and a random energy. Only trajectories for which the total $1s^2$ energy amounts to -2.9035 a.u. were kept and evolved in time.

The model was recently adapted to study the NSDI of He by short intense laser pulses [150]. This model has been extended to study the correlated electron emission in NSDI of Ar by few-cycle pulses ($a = 1.5$ a.u. and $b = 0.05$ a.u.) [151], as well as the double ionization of Xe and Ne by strong middle infrared laser pulses ($a = 2$ a.u. and $b = 0.01$ a.u.) [152] and ($a = 0.1$ a.u. and $b = 0.01$ a.u.) [97] respectively. In all cases, the nuclear charge is set as $Z_T = 2$.

2.5.8. The Gaussian Kernel Approximation

In this model, introduced by Guzmán et al. in 2009, the two electrons are assimilated to Gaussian density distributions for the calculation of the electron–electron repulsion [153]. The electron i , which is located at a position \mathbf{r}_i at time t , is represented by

$$f_i(\mathbf{r}, t) = \frac{1}{(2\pi)^{3/2}\sigma_r^3} \exp\left\{-\frac{|\mathbf{r} - \mathbf{r}_i|^2}{2\sigma_r^2}\right\}. \tag{19}$$

The potential felt by electron 1 due to electron 2 is calculated by assuming electron 1 as pointwise and electron 2 described by means of the Gaussian kernel:

$$V_{12}(\mathbf{r}_1, \mathbf{r}_2, t) = \int d\mathbf{r} f_2(\mathbf{r}, t) \frac{1}{|\mathbf{r} - \mathbf{r}_1|} = \frac{1}{r_{12}} \operatorname{erf}\left(\frac{r_{12}}{\sqrt{2}\sigma_r}\right). \tag{20}$$

This softening leads to stable two-electron He configurations. This model has been applied to $H^+ + \text{He}$ collisions, analyzing single ionization, single capture, double ionization, double capture and transfer ionization. This model provides a good description of one-electron processes but tends to overestimate the cross sections corresponding to two-electron transitions.

2.6. Explicit Multiple-Electron Descriptions of Atoms Beyond He: The Sequential Electrons and Independent Electrons CTMC

Atoms with a large number of electrons, such as Ne and Ar, have been considered by studying noninteracting independent electrons with binding energies such that they provide a picture of the ground state of the atom, or by nCTMC, in which electrons are sorted according to their sequential ionization energies [154,155]. Throughout the years, this model has been widely implemented in order to simulate light- and heavy-particle collisions on multielectronic atoms [156–159]. Unlike one-active-electron treatments based on the IPM model, this treatment allows tracking the momenta of all charged fragments for every collisional event and keeping a record of the deflection suffered by the projectile due to the interaction with all the particles of the target. The same comment applies for the independent electron version of nCTMC, in which the four-body model of the He atom is implemented, with both electrons initialized according to the first ionization value. As experimental studies of the transverse momentum acquired by the projectile became feasible at the end of the 1980s, the angular dependence of the fraction of double ionization to total ionization events showed a peak that is not reproduced by the independent particle model based on one-active-electron formulations. The independent electron version of nCTMC successfully reproduced the structure [155,160,161]. In subsequent years, this model was used to study the azimuthal angular dependence of the recoil ion and the electron emission in H^+ collisions on He at an impact energy of 500 keV [162].

2.7. Explicit Multiple-Electron Descriptions of Molecules

2.7.1. The H_2 Molecule

The first CTMC model for the treatment of collisions of multiply charged ions with H_2 molecules was performed by Meng et al. in the late 1980s, and it focused on the analysis of total cross sections for charge exchange and ionization for projectile charges in the range 1–10 and impact energies up to 1 MeV/u [163]. This five-body approach considered each target electron evolving under the influence of the two protons and a mean potential for the electron–electron interaction, which is calculated by means of a quantum mechanical variational wavefunction. This model allowed inferring the role of the autoionizing double-capture process for different projectile charges, that is, the dependence of the cross sections on the molecular orientation. In a subsequent study, (n,l)-state-selective cross sections were calculated and successfully benchmarked against the available data for He^{2+} projectiles [164].

An alternative approach was presented by Wood and Olson by the end of the 1990s to study the double ionization of H_2 by 3.6 MeV/u Se^{28+} and 1 GeV/u U^{92+} [165]. In this case, the H_2 molecule was initialized in terms of two independent hydrogen atoms united by means of a Morse potential. As one of the electrons is removed from the target (i.e., acquires a positive energy with respect to its parent nucleus), the interactions among all particles are turned on by means of a switching function. This model predicted that Thomas double scattering, in which an electron emitted from one center is scattered by the other, most likely proceeds when the molecular axis and the projectile velocity are perpendicular. This model has also been used to describe single-electron capture in He^+ collisions at intermediate- to low-impact energies [166]. In this case, very good agreement was found with the Bariloche COLTRIMS data for the n-state-selective capture cross sections, though some oscillations present in the experimental transverse momentum distribution for the recoil ion were not properly described by the theoretical model.

To our knowledge, the only classical attempts to consider the exact target Hamiltonian for H_2 was performed by Greenspan [167,168]. For the molecular ion H_2^+ , a four-body model was proposed by Hennecart and Pascale and was applied in $H_2^+ + H(1s)$ collisions [169]. These authors carefully analyzed the initial positions and momenta of all particles which prevents the autoionization of the molecule, thus allowing a stable simulation of the collision procedure.

2.7.2. The Molecular Multicenter—CTMC Approaches

In these types of models, the active electrons explicitly consider the different molecular centers in their dynamics. For the H₂O molecule, Illescas et al. calculated total cross sections for single ionization, single-electron capture, transfer ionization, double capture and double ionization following H⁺, He²⁺ and C⁶⁺ impact over an extensive impact energy range [12]. This study was carried out in the context of the IEV model by considering one active electron at a time to determine the reaction probabilities for the different orbitals. Their results were found to be in better agreement with the data compared with the IPM calculations performed in the Coulombic approximation.

In recent years, the model of Illescas has been extended by Jorge et al. by introducing a time-dependent screening in such a way that the number of frozen electrons at each center decreases if the ionization probability increases to values where multiple ionization becomes non-negligible [170]. The introduction of this correction was found to become relevant for increasing Z_p/v_p values. In a subsequent work, the authors extended the model and focused on the multinomial analysis of the multiple-electron capture processes, in the spirit of addressing the overestimation of the multiple-electron capture inherent in the IEM probabilistic scheme [171].

A strategy similar to Illescas' was implemented by Sarkadi to study the ionization of gas-phase uracil by means of protons and heavy ions [172,173]. In this one-active-electron treatment, the electron interacts with all the nuclei conforming the molecule, and cross sections are determined by separately analyzing all the cross sections corresponding to each molecular orbital. Cross sections at the total, single-differential and double-differential levels were benchmarked against the reported data, as well as other theoretical approaches.

A many-electron–multicenter classical trajectory Monte Carlo model was introduced by Cariatore and was tested in charge-exchange studies involving projectiles with charges from +3 to +10 and the CO molecule [174]. In this model, eight electrons were randomly sorted in the energetically allowed region, thus considering two electrons for the 3σ orbital, four for the 1π orbital and two the 2σ orbital. Total and state-selective charge-exchange cross sections were presented and compared with the Jet Propulsion Laboratory data, leading to good overall agreement.

2.7.3. The Classical Overbarrier—CTMC Approach

This model was introduced by Abbas et al. in 2008 in order to describe the single and multiple ionization of biological molecules by protons and α-particle impact [175]. In this approach, the target electrons are treated as virtual particles and are incorporated in the collision dynamics once they are in condition to be removed from the target. In practical terms, this amounts to keeping continuous track (i.e., for each time step $\Delta t \cong 10^{-2}$ a.u. of the projectile) of the potential seen by the virtual electron, and that is given by

$$V(\mathbf{r}_1) = -\frac{Z_p}{|\mathbf{r}_1 - \mathbf{R}| + a} - \frac{Z_T + 1}{r_1 + a}. \quad (21)$$

The parameter a was introduced as a numerical cut-off to avoid singularities during the simulation. Molecular targets are therefore treated in a Coulomb single-center approximation. The electron creation is determined by two simultaneous criteria:

- The virtual electron energy must overcome the potential saddle barrier.
- A random number $\delta \in (0, 1)$ is sorted and compared with the ratio $\Delta t/T_e$, T_e being the classical electron orbital period. If $\delta < \Delta t/T_e$, the electron is created and randomly located within a sphere of a few atomic units of radius centered on the target.

The process is repeated, incorporating in the potential for the second, third, etc. virtual electrons the terms associated with the previously released electrons. Total cross sections for the single ionization of DNA and RNA bases by energetic H⁺, He²⁺ and C⁶⁺ projectiles were also studied with this method [176]. An IEM adaptation of this model was also introduced in [177] to study, at the total cross-section level, the ionization of molecules of biological interest by proton impact. In this case, only one virtual electron was considered,

as well as double ionization and transfer ionization, calculated by means of the IEM probabilistic scheme.

2.7.4. The Dynamical Adaptive CTMC Model

This model was introduced by Bachi et al. in 2019 with the aim of compensating the inherent limitations of the independent electrons and the sequential electron models [178]. In the former, electrons are bound with fixed ionization potentials, providing a picture of the ground-state valence molecular orbitals. In this model, the electron density seen by the projectile is in principle correct, but the energy deposition necessary for multiple-electron removal is underestimated. In contrast, the sequential electron model, in which the electrons are sorted according to the vertical ionization energies, guarantees that the proper amount of energy is deposited in the target during any multiple-electron removal process. The drawback in this case is that the target electron density seen by the projectile for the valence molecular orbitals is incorrect.

The present scheme merges both models in a dynamical way. At the beginning of the simulation, the electrons are sorted by means of the independent electron model. Each electron is associated with a particular molecular orbital of the A molecule ground state, with its corresponding binding energy. In every step during the simulation, the energy of the electrons with respect to their parent nucleus is checked. As one electron acquires a positive energy, the other bound electrons are resorted with the ionization potentials corresponding to the A^+ ion by assuming a vertical transition for the molecule. The target nuclear charge is also increased by one unit, reflecting the increase in the strength of the interaction among the bound electrons and their parent nucleus. This procedure is repeated as new electrons are emitted from the target. Total net cross sections and single-differential ionization cross sections in energy and angle for H_2O ionization by bare-ion impact were studied in ref. [178] and compared with the available experimental and theoretical data [179,180]. The analysis of the separate contributions of the single-ionization and multiple-ionization channels to the electronic spectra indicates that multiple ionization dominates the fast electron emission, while single ionization dominates the emission of low-energy electrons. Besides, these contributions can be related to different ranges of impact parameters.

This methodology has been recently extended to analyze the single and multiple ionization of uracil by C^6 projectiles at MeV/u impact energies [181]. In the study, 21 molecular orbitals were initialized following the statistical procedure described above for the molecular multicenter CTMC approach by sorting each electron for each trajectory over the possible different centers of a given molecular orbital following the Mulliken population scheme. The energy of each electron relative to its parent atomic core, and to the rest of the atomic centers in their corresponding molecular orbital, is tracked at all times. Once these relative energies become positive, the electron is assumed to have been emitted, and the adaptive scheme is implemented as previously described. Very good agreement was obtained with the available data at the total, singly differential and doubly differential levels.

2.8. Line Emission Cross Sections following Charge Exchange in Collisions Involving Highly Charged Projectiles and Multielectronic Targets

Finally, we would like to point out that either for multielectronic atoms or molecules, multiple-electron removal gains relevance with increasing projectile charge. Multiple-electron capture, in particular, represents a challenge for classical methodologies, since the consecutive relaxation process strongly depends on the interelectronic correlation. As multiple-electron capture populates high-lying n-levels, the use of time-dependent collisional radiative models becomes impractical [182,183] and simpler, though still physically sound, strategies should be invoked. One of them is the method proposed by Machacek et al. that considers all the radiative and autoionization rates and, via a Monte Carlo procedure, determines the decay routes until an ion in its ground state is obtained [184]. Another

one is the phenomenological stabilization scheme developed by Ali et al. [185], which was successfully implemented in subsequent studies by many other groups [174,186,187] and that, due to its underlying conceptual richness, we now summarize:

- Multiply excited states dominantly stabilized via multiple Auger processes.
- Only two-electron Auger processes are considered.
- Transitions involving electrons in the same shell proceed first. If several electrons are in different shells, the Auger process involves the two electrons which are energetically closer.
- Each Auger transition proceeds with the unit probability to the nearest continuum limit. The decaying electron falls to a well-established n level according to the energy conservation equation.
- If the new configuration still provides a multiple-excited state involving more than two electrons, these rules are applied again until only two electrons remain bound to the projectile.
- If a cascading process leads to an asymmetric double-excited state, the event is characterized as double radiative decay. Otherwise, a final Auger process takes place, and the event is characterized as a single charge exchange.

There is still one issue that should be addressed, and it is how the l -values are handled in the decay process. As already stated above, CTMC studies by Olson showed that during the capture process, the electron tries to preserve its orbital eccentricity [35]. Therefore, by fulfilling this condition during the relaxation process, i.e., $l_f = l_i(n_f/n_i)$, the risk of having unphysical l_f values is ruled out, providing at the same time a unique criterion for the procedure [117,174].

In Figure 7, we present a schematic diagram of two punctual Auger decay processes analyzed by means of the Ali decay scheme during a sequential CTMC simulation of $\text{Ar}^{18} + \text{Ar}$ collisions at an impact energy of 4 keV/u [188]. In the nCTMC model, eight electrons (the whole M shell) were explicitly considered. The selected events correspond to the capture of seven electrons by the bare projectile and lead to either autoionizing multiple capture or double radiative decay, depending on their initial n -level population. These punctual cases are considered representative, since multiple-electron capture was found in this case to be responsible for 50–60% of the resulting X-ray spectra. Moreover, this method led to very good agreement with the 4 keV/u Ne^{10+} , Ar^{18+} and $\text{Kr}^{36+} + \text{Ar}$ line emission cross sections measured at the NIST-EBIT [189], as well as with the 18 eV/u and 218/eV $\text{Ar}^{18+} + \text{Ar}$ line emission cross sections measured at the Berlin-EBIT [190]. An interesting feature in the resulting emission spectra is that in contrast to the autoionizing multiple capture, the double radiative decay leads to a low-energy shoulder in the Ly- α structure for Ne^{10+} and Ar^{18+} projectiles, which evolves into a well-separated peak for Kr^{36+} , thus providing clear visual evidence of the relative contribution of the double radiative decay.

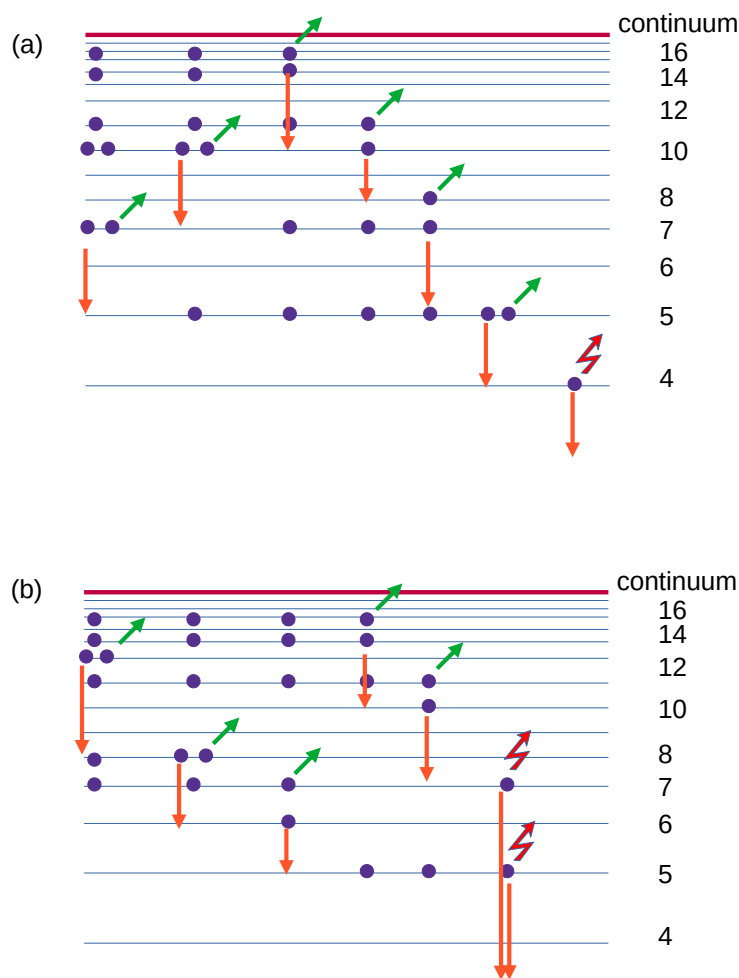


Figure 7. Schematic diagram of Auger decay processes following multiple-electron capture events in an 8-electron sequential CTMC simulation of 4 keV/u $\text{Ar}^{18} + \text{Ar}$ collisions: (a) Autoionizing multiple capture; (b) double radiative decay. In these figures, the temporal sequence of events runs from left to right. Green arrows represent electrons emitted to the continuum; orange arrows represent electronic transitions to inner discrete levels; and red zigzag arrows represent photons emitted during the de-excitation process.

3. Conclusions and Perspectives

During the past five decades, the CTMC model has established itself as a versatile tool to study collision processes at the quantum scale. Despite the fact that conclusions based on classical collisional mechanics should be taken with caution in the quantum mechanical domain, the CTMC method in this period has provided accurate data for a wide variety of processes, including heavy-ion, light-particles and laser-field collisions. Not being limited by a basis set size, the method naturally deals with very highly charged projectiles and predicts capture cross sections to very high-lying excited states.

Its different variations, developed during the lapse described in this review to improve the description of atomic and molecular targets, were stimulated by a new generation of experimental devices, such as reaction microscopes, the introduction of the COLTRIMS and MOTRIMS techniques and the advance of the electron beam ion (EBIT) traps. The generated data have benchmarked the novel data and provide, in parallel to quantum mechanical methods, theoretical support for new experimental endeavors.

After five decades, and in the immediate future, the CTMC methods face new challenges, either from the basic science perspective or in diverse fields, such as the ther-

monuclear fusion reactor program, hadrontherapy and space weather, where ample sets of reliable cross sections are needed in transport codes.

Funding: This work has been supported by Grant No. PGI-24/F084, Secretaría General de Ciencia y Tecnología, Universidad Nacional del Sur.

Data Availability Statement: The published data are available from the author upon reasonable request.

Acknowledgments: The author would like to thank Ron Olson for his long standing collaboration and support and his collaborators at IFISUR, N. D. Cariatore, N. Bachi, E. Acebal and S. Martínez for fruitful discussions.

Conflicts of Interest: The author declares no conflicts of interest.

References

1. Hirschfelder, J.; Eyring, H.; Topley, B. Reactions of hydrogen molecules and atoms. *J. Chem. Phys.* **1936**, *4*, 170–177. [[CrossRef](#)]
2. Wall, F.T.; Hiller, L.A., Jr.; Mazur, J. Statistical Computation of Reaction Probabilities. *J. Chem. Phys.* **1958**, *29*, 255–263. [[CrossRef](#)]
3. Wall, F.T.; Hiller, L.A. Jr.; Mazur, J. Statistical Computation of Reaction Probabilities II. *J. Chem. Phys.* **1961**, *35*, 1284–1289. [[CrossRef](#)]
4. Wall, F.T.; Porter, R. Sensitivity of exchange reaction probabilities to the potential energy surface. *J. Chem. Phys.* **1963**, *39*, 3112–3117. [[CrossRef](#)]
5. Karplus, M.; Porter, R.N.; Sharma, R.D. Exchange reactions with activation energy I. Simple barrier potential for (H,H₂). *J. Chem. Phys.* **1965**, *39*, 3259–3287. [[CrossRef](#)]
6. Abrines, R.; Percival, I.C. Classical theory of charge transfer and ionization of hydrogen atoms by protons. *Proc. Phys. Soc.* **1966**, *88*, 861–872. [[CrossRef](#)]
7. Abrines, R.; Percival, I.C. A generalized correspondence principle and proton-hydrogen collisions. *Proc. Phys. Soc.* **1966**, *88*, 873–883. [[CrossRef](#)]
8. Olson, R.E.; Salop, A. Charge-transfer and impact-ionization cross sections for fully and partially stripped positive ions colliding with atomic hydrogen. *Phys. Rev. A* **1977**, *16*, 531–541. [[CrossRef](#)]
9. Olson, R.E. Multiple-ionisation cross sections for highly stripped ions colliding with He, Ne and Ar. *J. Phys. B Atom. Molec. Phys.* **1979**, *12*, 1843–1849. [[CrossRef](#)]
10. Peach, G.; Willis, S.L.; McDowell, M.R.C. The classical theory of charge transfer and ionization processes in collisions between complex atomic ions. *J. Phys. B At. Mol. Phys.* **1985**, *18*, 3921–3937. [[CrossRef](#)]
11. Reinhold, C.O.; Falcón, C.A. Classical ionization and charge-transfer cross sections for H⁺ + He and H⁺ + Li⁺ collisions with consideration of model interactions. *Phys. Rev. A* **1986**, *33*, 3859–3866. [[CrossRef](#)] [[PubMed](#)]
12. Illescas, C.; Errea, L.F.; Méndez, L.; Pons, B.; Rabadán, I.; Riera, A. Classical treatment of ion-H₂O collisions with a three-center model potential. *Phys. Rev. A* **2011**, *83*, 052704. [[CrossRef](#)]
13. Garvey, R.H.; Jackman, C.H.; Green, A.E.S. Independent-particle-model potentials for atoms and ions with $36 < Z \leq 54$ and a modified Thomas-Fermi atomic energy formula. *Phys. Rev. A* **1975**, *12*, 1144–1152.
14. Zhang, H.; Wang, J.G.; He, B.; Qiu, Y.B. Charge exchange and ionization in hydrogen atom-fully stripped ion collisions in Debye plasmas. *Phys. Plasmas* **2007**, *14*, 053505. [[CrossRef](#)]
15. Cariatore, N.D.; Otranto, S. Strong sensitivity of X-ray emission lines following charge exchange between highly charged ions and H(1s) in weakly screened media. *Phys. Rev. A* **2015**, *92*, 052705. [[CrossRef](#)]
16. Acebal, E.; Martínez, S.H.; Otranto, S. Differential Analysis of the Positron Impact Ionization of Hydrogen in Debye Plasmas. *Atoms* **2023**, *11*, 15. [[CrossRef](#)]
17. Zhang, L.; Zhao, X.; Wan, J.; Xiao, G.; Duan, W.; Qi, X.; Yang, L. Dynamics of the fully stripped ion-hydrogen atom charge exchange process in dense quantum plasmas. *Phys. Plasmas* **2014**, *21*, 093302. [[CrossRef](#)]
18. Eichenauer, D.; Grün, N.; Scheid, W. Classical trajectory calculations for H⁺-H collisions with the Wigner function as initial phase space distribution. *J. Phys. B At. Mol. Phys.* **1981**, *14*, 3929–3941. [[CrossRef](#)]
19. Hardie, D.J.W.; Olson, R.E. Charge transfer and ionisation processes involving multiply charged ions in collision with atomic hydrogen. *J. Phys. B At. Mol. Phys.* **1983**, *16*, 1983–1996. [[CrossRef](#)]
20. Illescas, C.; Riera, A. Classical study of single-electron capture and ionization processes in A^{q+} + (H,H₂) collisions. *Phys. Rev. A* **1999**, *60*, 4546–4560. [[CrossRef](#)]
21. Cariatore, N.D.; Otranto, S.; Olson, R.E. Classical description of H(1s) and H*(n = 2) for cross-section calculations relevant to charge-exchange diagnostics. *Phys. Rev. A* **2015**, *91*, 042709. [[CrossRef](#)]
22. Cohen, J.S. Classical phase-space distributions for atomic hydrogen collisions. *J. Phys. B At. Mol. Phys.* **1985**, *18*, 1759–1769. [[CrossRef](#)]
23. Cariatore, N.D.; Otranto, S.; Olson, R.E. Reply to “Comment on ‘Classical description of H(1s) and H*(n = 2) for cross-section calculations relevant to charge-exchange diagnostics’”. *Phys. Rev. A* **2016**, *93*, 066702. [[CrossRef](#)]

24. Fowler, R.H. The statistical theory of dissociation and ionization by collision, with applications to the capture and loss of electrons by α -particles. *Math. Proc. Camb. Phil. Soc.* **1924**, *22*, 253–272. [[CrossRef](#)]
25. Rutherford, E. The capture and loss of electrons by α -particles. *Phil. Mag.* **1924**, *47*, 277–303. [[CrossRef](#)]
26. Oppenheimer, J.R. On the quantum theory of the capture of electrons. *Phys. Rev.* **1928**, *31*, 349–356. [[CrossRef](#)]
27. Bohr, N.; Lindhard, J. Electron capture and loss by heavy ions penetrating through matter. *K. Dan. Vid. Seel. Mat. Phys. Medd.* **1954**, *28*, 1–30.
28. Grozdanov, T.P. Classical model for electron capture in collisions of highly charged, fully stripped ions with hydrogen atoms. *J. Phys. B At. Mol. Phys.* **1980**, *13*, 3835–3847. [[CrossRef](#)]
29. Ryufuku, H.; Sasaki, K.; Watanabe, T. Oscillatory behavior of charge transfer cross sections as a function of the charge of the projectiles in low-energy collisions. *Phys. Rev. A* **1980**, *21*, 745–750. [[CrossRef](#)]
30. Bárány, A.; Astner, G.; Cederquist, H.; Danared, H.; Hult, H.; Hvelplund, P.; Johnson, A.; Knudsen, H.; Liljeby, L.; Resnfelt, K.-G. Absolute cross sections for multi-electron processes in low energy Ar^{q+} -Ar collisions: Comparison with theory. *Nucl. Instr. Methods B* **1985**, *9*, 397–399. [[CrossRef](#)]
31. Niehaus, A. A classical model for multiple-electron capture in slow collisions of highly charged ions with atoms. *J. Phys. B At. Mol. Phys.* **1986**, *19*, 2925–2937. [[CrossRef](#)]
32. Burdörfer, J.; Morgenstern, R.; Niehaus, A. Angular momentum distribution in the classical over-barrier model for electron capture into highly charged slow projectiles. *J. Phys. B At. Mol. Phys.* **1986**, *19*, L507–L513.
33. Olson, R.E.; Berkner, K.H.; Graham, W.G.; Pyle, R.V.; Schlachter, A.S.; Stearns, J.W. Charge exchange dependence of electron loss from H by collisions with heavy, highly stripped projectiles. *Phys. Rev. Lett.* **1978**, *41*, 163–166. [[CrossRef](#)]
34. Olson, R.E. Ion-Rydberg atom collision cross sections. *J. Phys. B At. Mol. Phys.* **1980**, *13*, 483–492. [[CrossRef](#)]
35. Olson, R.E. n, l distribution in $A^{q+} + H$ electron capture collisions. *Phys. Rev. A* **1981**, *24*, 1726–1732. [[CrossRef](#)]
36. Becker, R.L.; McKellar, A.D. Theoretical initial l dependence of ion-Rydberg-atom collision cross sections. *J. Phys. B At. Mol. Phys.* **1984**, *17*, 3923–3942. [[CrossRef](#)]
37. Igenbergs, K. Calculation of Cross Sections Relevant for Diagnostics of Hot Fusion Plasmas. Ph.D. Thesis, Vienna University of Technology, Vienna, Austria, 2011.
38. Igenbergs, K.; Schweinzer, J.; Veiter, A.; Perneczky, L.; Frühwirth, E.; Wallerberger, M.; Olson, R.E.; Aumayr, F. Charge exchange and ionization in N^{7+-} , N^{6+-} , C^{6+-} -H ($n = 1, 2$) collisions studied systematically by theoretical approaches. *J. Phys. B At. Mol. Opt. Phys.* **2012**, *45*, 065203. [[CrossRef](#)]
39. Payne, C. Stellar Atmospheres. A Contribution to the Observational Study of High Temperature in the Reversing Layers of Stars. Ph.D. Thesis, Harvard Observatory Monographs, Cambridge, MA, USA, 1925.
40. Bethe, H. Zur Theorie des Durchgangs schneller Korpuskularstrahlen durch Materie. *Ann. Phys.* **1930**, *5*, 325–400. [[CrossRef](#)]
41. Blauth, E. Zur Energieverteilung der von Protonen in Gasen ausgelösten Sekundärelektronen. *Z. Physik* **2019**, *147*, 228–240. [[CrossRef](#)]
42. Moe, D.; Petsch, E. Energy Spectrum of Electrons Emitted from Gases Bombarded by Positive Ions. *Phys. Rev.* **1958**, *110*, 1358–1361. [[CrossRef](#)]
43. Kuyatt, C.E.; Jorgensen, T., Jr. Energy and Angular Dependence of the Differential Cross Section for Production of Electrons by 50–100 keV Protons in Hydrogen Gas. *Phys. Rev.* **1963**, *130*, 1444–1455. [[CrossRef](#)]
44. Rudd, M.E.; Jorgensen, T., Jr. Energy and Angular Distribution of Electrons Ejected from Hydrogen and Helium Gas by Protons. *Phys. Rev.* **1963**, *131*, 666–675. [[CrossRef](#)]
45. Rudd, M.E.; Sautter, C.A.; Bailey, C.L. Energy and angular distributions of electrons ejected from hydrogen and helium by 100- to 300-keV protons. *Phys. Rev.* **1966**, *151*, 20–27. [[CrossRef](#)]
46. Rudd, M.E.; Jorgensen, T., Jr.; Volz, D.J. Electron Energy Spectrum from Ar^{+} -Ar and H^{+} -Ar Collisions. *Phys. Rev.* **1966**, *151*, 28–31. [[CrossRef](#)]
47. Crooks, G.B.; Rudd, M.E. Experimental evidence for the mechanism of charge transfer into continuum states. *Phys. Rev. Lett.* **1970**, *25*, 1599–1601. [[CrossRef](#)]
48. Barrachina, R.O. Final-state interaction theory of cusp formation. *Nucl. Inst. Meth. Phys. Res. B* **1997**, *124*, 198–205. [[CrossRef](#)]
49. Garibotti, C.R.; Miraglia, J.E. Ionization and electron capture to the continuum in the H^{+} -hydrogen-atom collision. *Phys. Rev. A* **1980**, *21*, 572–580. [[CrossRef](#)]
50. Bernardi, G.C.; Suárez, S.; Fainstein, P.D.; Garibotti, C.R.; Meckbach, W.; Focke, P. Two-center effects in electron emission in ${}^3\text{He}^{2+}$ -He and H^{+} -He collisions at intermediate energies. *Phys. Rev. A* **1989**, *40*, 6863–6872. [[CrossRef](#)]
51. Fainstein, P.D.; Ponce, V.H.; Rivarola, R.D. Two-centre effects in ionization by ion impact. *J. Phys. B At. Mol. Opt. Phys.* **1991**, *24*, 3091–3119. [[CrossRef](#)]
52. Gulyas, L.; Fainstein, P.D.; Salin, A. CDW-EIS theory of ionization by ion impact with Hartree-Fock description of the target. *J. Phys. B At. Mol. Opt. Phys.* **1995**, *28*, 245–257. [[CrossRef](#)]
53. Gulyas, L.; Fainstein, P.D. CDW theory of ionization by ion impact with a Hartree-Fock-Slater description of the target. *J. Phys. B At. Mol. Opt. Phys.* **1998**, *31*, 3297–3305. [[CrossRef](#)]
54. Reinhold, C.O.; Olson, R.E. Classical two-center effects in ejected-electron spectra from p^{+} , p^{-} and He^{2+} +He collisions at intermediate energies. *Phys. Rev. A* **1989**, *39*, 3861–3870. [[CrossRef](#)]

55. Barrachina, R.O.; Courbin, C. Cusp formation in classical trajectory Monte Carlo calculations of ion-impact ionization collisions. *J. Phys. B At. Mol. Opt. Phys.* **2002**, *35*, 3157–3165. [[CrossRef](#)]
56. Tórkési, K.; Sarkadi, L.; Mukoyama, T. Model calculation of the electron capture to the continuum peak of neutral projectile impact. *J. Phys. B At. Mol. Opt. Phys.* **1997**, *30*, L123–L129. [[CrossRef](#)]
57. Illescas, C.; Pons, B.; Riera, A. Classical description of the electron capture to the continuum cusp formation in ion-atom collisions. *Phys. Rev. A* **2002**, *65*, 030703(R). [[CrossRef](#)]
58. Sarkadi, L.; Lugosi, L.; Tórkési, K.; Gulyas, L.; Kövér, Á. Study of the transfer ionization process by observing of the electron cusp in 100–300 keV He²⁺+He collisions. *J. Phys. B At. Mol. Opt. Phys.* **2001**, *34*, 4901. [[CrossRef](#)]
59. Moshhammer, R.; Unverzagt, M.; Schmitt, W.; Ullrich, J.; Schmidt-Böcking, H. A 4 π recoil-ion electron momentum analyzer: A high-resolution “microscope” for the investigation of the dynamics of atomic, molecular and nuclear reactions. *Nucl. Instr. Methods B* **1996**, *108*, 425–445. [[CrossRef](#)]
60. Weber, T.H.; Khayyat, K.H.; Dörner, R.; Rodríguez, V.D.; Mergel, V.; Jagutzki, O.; Schmidt, L.; Müller, K.A.; Afaneh, F.; Gonzalez, A.; et al. Abrupt rise of the longitudinal recoil ion momentum distribution for ionizing collisions. *Phys. Rev. Lett.* **2001**, *86*, 224–227. [[CrossRef](#)]
61. Fainstein, P.D. Longitudinal electron momentum distributions in single ionization of helium by light particles. *J. Phys. B At. Mol. Opt. Phys.* **1996**, *29*, L763–L767. [[CrossRef](#)]
62. Dörner, R.; Mergel, V.; Zhaoyuan, L.; Ullrich, J.; Spielberger, L.; Olson, R.E.; Schmidt-Böcking, H. Three-body final-state momentum distributions for swift H⁺ and He²⁺ on He collisions. *J. Phys. B At. Mol. Opt. Phys.* **1995**, *28*, 435–444. [[CrossRef](#)]
63. Wood, C.J.; Olson, R.E. Three-body collision dynamics for single ionization of helium by protons and antiprotons. *J. Phys. B At. Mol. Opt. Phys.* **1996**, *29*, L257–L262. [[CrossRef](#)]
64. Ehrhardt, H.; Schulz, M.; Tekaas, T.; Willmann, K. Ionization of helium: Angular correlation of the scattered and the emitted electrons. *Phys. Rev. Lett.* **1969**, *22*, 89–92. [[CrossRef](#)]
65. Amaldi, U., Jr.; Egidi, A.; Marcoreno, R.; Pizzella, G. Use of a two channeltron coincidence in a new line of research in atomic physics. *Rev. Sci. Instrum.* **1969**, *40*, 1001–1004. [[CrossRef](#)]
66. Ullrich, J.; Moshhammer, R.; Dorn, A.; Dörner, R.; Schmidt, L.P.H.; Schmidt-Böcking, H. Recoil-ion and electron momentum spectroscopy: Reaction-microscopes. *Rep. Prog. Phys.* **2003**, *66*, 1463–1545. [[CrossRef](#)]
67. de Lucio, O.G.; Gavin, J.; DuBois, R.D. Differential electron emission for single and multiple ionization of argon by 500 eV positrons. *Phys. Rev. Lett.* **2006**, *97*, 243201. [[CrossRef](#)] [[PubMed](#)]
68. de Lucio, O.G.; Otranto, S.; Olson, R.E.; DuBois, R.D. Triply Differential Single Ionization of Argon: Charge Effects for Positron and Electron Impact. *Phys. Rev. Lett.* **2010**, *104*, 163201. [[CrossRef](#)]
69. Madison, D.H. Angular distribution of electrons ejected from helium by proton impact. *Phys. Rev. A* **1973**, *8*, 2449–2455. [[CrossRef](#)]
70. Brauner, M.; Briggs, J.S.; Klar, H. Triply-differential cross sections for ionisation of hydrogen atoms by electrons and positrons. *J. Phys. B At. Mol. Opt. Phys.* **1989**, *22*, 2265–2287. [[CrossRef](#)]
71. Berakdar, J.; Briggs, J.S. Three-body Coulomb continuum problem. *Phys. Rev. Lett.* **1994**, *72*, 3799–3802. [[CrossRef](#)]
72. Berakdar, J. Approximate analytical solution of the quantum-mechanical three-body Coulomb continuum problem. *Phys. Rev. A* **1996**, *53*, 2314–2326. [[CrossRef](#)]
73. Jones, S.; Madison, D.H. Evidence of initial-state two-center effects for (*e, 2e*) reactions. *Phys. Rev. Lett.* **1998**, *81*, 2886–2889. [[CrossRef](#)]
74. Jones, S.; Madison, D.H. Ionization of hydrogen atoms by fast electrons. *Phys. Rev. A* **2000**, *62*, 042701. [[CrossRef](#)]
75. Otranto, S. Initial state correlation in the electron-impact ionization of argon. *Phys. Rev. A* **2009**, *79*, 012705. [[CrossRef](#)]
76. Acebal, E.; Otranto, S. Continuum-distorted-wave eikonal-initial-state of the electron-impact ionization of H₂O at low impact energies. *Phys. Rev. A* **2018**, *98*, 012703. [[CrossRef](#)]
77. Colgan, J.; Foster, M.; Pindzola, M.S.; Bray, I.; Stelbovics, A.T.; Fursa, D.V. Triple differential cross sections for the electron-impact ionization of helium at 102 eV incident energy. *J. Phys. B At. Mol. Opt. Phys.* **2009**, *42*, 145002. [[CrossRef](#)]
78. Bray, I.; Fursa, D.V.; Kadyrov, A.S.; Stelbovics, A.T. Single ionization of helium by electron impact. *Phys. Rev. A* **2010**, *81*, 062704. [[CrossRef](#)]
79. Wang, Y.; Zatsarinny, O.; Bartschat, K. B-spline R-matrix-with-pseudostates for electron-impact excitation and ionization of carbon. *Phys. Rev. A* **2013**, *87*, 012704. [[CrossRef](#)]
80. Schultz, D.R. Comparison of single-electron removal processes in collisions of electrons, positrons, protons and antiprotons with hydrogen and helium. *Phys. Rev. A* **1989**, *40*, 2330–2334. [[CrossRef](#)]
81. Schultz, D.R.; Reinhold, C.O.; Olson, R.E. Large-angle scattering in positron-helium and positron-krypton collisions. *Phys. Rev. A* **1989**, *40*, 4947–4958. [[CrossRef](#)]
82. Schultz, D.R.; Meng, L.; Olson, R.E. Classical description and calculation of ionization in collisions of 100 eV electrons and positrons with He and H₂. *J. Phys. B At. Mol. Opt. Phys.* **1992**, *25*, 4601–4618. [[CrossRef](#)]
83. Fiol, J.; Rodríguez, V.D.; Barrachina, R.O. Electron capture to the continuum by proton and positron impact. *J. Phys. B At. Mol. Opt. Phys.* **2001**, *34*, 933–944. [[CrossRef](#)]
84. Fiol, J.; Barrachina, R.O. Dynamical orientation effects in the ionization of atoms and molecules by positron impact. *J. Phys. B At. Mol. Opt. Phys.* **2009**, *42*, 231004. [[CrossRef](#)]

85. Fiol, J.; Barrachina, R.O. Continuum orientation phenomena in ionization by positron impact. *J. Phys. B At. Mol. Opt. Phys.* **2011**, *44*, 075205. [[CrossRef](#)]
86. Tókési, K.; Köver, Á. Electron capture to the continuum at 54.4 eV positron–argon atom collisions. *J. Phys. B At. Mol. Opt. Phys.* **2000**, *33*, 3067–3077. [[CrossRef](#)]
87. Bachi, N.; Otranto, S.; Tókési, K. Electron-impact ionization of carbon. *Atoms* **2023**, *11*, 16. [[CrossRef](#)]
88. Balutška, A.; Udem, T.H.; Uiberacker, M.; Hentschel, M.; Goulielmakis, E.; Gohle, C.H.; Holzwarth, R.; Yakovlev, V.S.; Scrinzi, A.; Hänsch, T.W.; et al. Attosecond control of electronic processes by intense light fields. *Nature* **2003**, *421*, 611–615. [[CrossRef](#)]
89. Liu, X.; Rottke, H.; Eremina, E.; Sandner, W.; Goulielmakis, E.; Keeffe, K.O.; Lezius, M.; Krausz, F.; Lindner, F.; Schätzel, M.G.; et al. Nonsequential double ionization at the single-optical-cycle limit. *Phys. Rev. A* **2004**, *93*, 263001. [[CrossRef](#)]
90. Johnson, N.G.; Herrwerth, O.L.; Wirth, A.; De, S.; Ben-Itzhak, I.; Lezius, M.; Bergues, B.; Kling, M.F.; Senftleben, A.; Schröter, A.; et al. Single-shot carrier-envelope-phase-tagged ion-momentum imaging of nonsequential double ionization of argon in intense 4-fs laser fields. *Phys. Rev. A* **2011**, *83*, 013412. [[CrossRef](#)]
91. Bergues, B.; Kübel, M.; Johnson, N.G.; Fischer, B.; Camus, N.; Betsch, K.J.; Herrwerth, W.; Senftleben, A.; Max Sayler, A.; Rathje, T.; et al. Attosecond tracing of correlated electron-emission in non-sequential double ionization. *Nat. Commun.* **2012**, *3*, 813. [[CrossRef](#)]
92. Kübel, M.; Kling, N.G.; Betsch, K.J.; Camus, N.; Kaldun, A.; Kleineberg, U.; Ben-Itzhak, I.; Jones, R.R.; Paulus, G.G.; Pfeifer, T.; et al. Nonsequential double ionization of N₂ in a near-single-cycle laser pulse. *Phys. Rev. A* **2013**, *88*, 023418. [[CrossRef](#)]
93. Kübel, M.; Kling, N.G.; Betsch, K.J.; Camus, N.; Kaldun, A.; Kleineberg, U.; Ben-Itzhak, I.; Jones, R.R.; Paulus, G.G.; Pfeifer, T.; et al. Complete characterization of single-cycle double ionization of argon from the nonsequential to the sequential ionization regime. *Phys. Rev. A* **2016**, *93*, 053422. [[CrossRef](#)]
94. Kubel, M.; Arbeiter, M.; Burger, C.; Kling, N.G.; Pischke, T.; Moshhammer, R.; Fennel, T.; Kling, M.F.; Bergues, B. Phase- and intensity-resolved measurements of above threshold ionization by few-cycle pulses. *J. Phys. B At. Mol. Opt. Phys.* **2018**, *51*, 134007. [[CrossRef](#)]
95. Walker, B.; Sheehy, B.; DiMauro, L.F.; Agostini, P.; Schafer, K.J.; Kulander, K.C. Precise measurement of strong field double ionization of helium. *Phys. Rev. Lett.* **1994**, *73*, 1227–1230. [[CrossRef](#)] [[PubMed](#)]
96. Becker, W.; Liu, X.; Eberly, J.H. Theories of photoelectron correlation in laser-driven multiple atomic ionization. *Rev. Mod. Phys.* **2012**, *84*, 1011–1043. [[CrossRef](#)]
97. Chen, X.; Ruiz, C.; He, F.; Zhang, J. Mapping initial transverse momenta of tunnel-ionized electrons to rescattering double ionization in nondipole regimes. *Opt. Expr.* **2020**, *28*, 14894–14896. [[CrossRef](#)]
98. Lin, K.; Chen, X.; Eckart, S.; Jiang, H.; Hartung, A.; Trabert, D.; Fehre, K.; Rist, J.; Schmidt, L.P.H.; Schöffler, M.; et al. Magnetic-field effect as a tool to investigate electron correlation in strong-field ionization. *Phys. Rev. Lett.* **2022**, *128*, 113201. [[CrossRef](#)] [[PubMed](#)]
99. Arbó, D.G.; Persson, E.; Dimitriou, K.I.; Burgdörfer, J. Carrier-envelope phase dependence in atomic ionization by short-laser pulses. *Nucl. Instr. Methods B* **2009**, *267*, 330–333. [[CrossRef](#)]
100. Grum-Grzhimailo, A.N.; Abeln, B.; Bartschat, K.; Weflen, D.; Urness, T. Ionization of atomic hydrogen in strong infrared laser fields. *Phys. Rev. A* **2010**, *81*, 043408. [[CrossRef](#)]
101. Djiokep, J.M.N.; Hu, S.X.; Jiang, W.; Peng, L.; Starace, A. Enhanced asymmetry in few-cycle attosecond pulse ionization of He in the vicinity of autoionizing resonances. *New J. Phys.* **2012**, *14*, 095010. [[CrossRef](#)]
102. Figueira de Morisson Faria, C.; Liu, X.; Sanpera, A.; Lewenstein, M. Classical and quantum-mechanical treatments of nonsequential double ionization with few-cycle laser pulses. *Phys. Rev. A* **2004**, *70*, 043406. [[CrossRef](#)]
103. Cohen, J.S. Reexamination of the over-the-barrier and tunneling ionization of the hydrogen atom in an intense field. *Phys. Rev. A* **2001**, *64*, 043412. [[CrossRef](#)]
104. McGuire, J.H.; Weaver, L. Independent electron approximation for atomic scattering by heavy particles. *Phys. Rev. A* **1977**, *16*, 41–47. [[CrossRef](#)]
105. Olson, R.E. Electron-capture and impact-ionization cross sections for multiply charged ions colliding with helium. *Phys. Rev. A* **1978**, *18*, 2464–2469. [[CrossRef](#)]
106. Olson, R.E.; Gay, T.J. Dynamics of Antimatter-Atom Collisions. *Phys. Rev. Lett.* **1988**, *61*, 302–305. [[CrossRef](#)] [[PubMed](#)]
107. Crothers, D.S.F.; McCarroll, R. Correlated continuum distorted-wave resonant double electron capture in He²⁺-He collisions. *J. Phys. B At. Mol. Phys.* **1987**, *20*, 2835–2842. [[CrossRef](#)]
108. Liamsuwan, T.; Nikjoo, H. Cross sections for bare and dressed carbon ions in water and neon. *Phys. Med. Biol.* **2013**, *58*, 641–672. [[CrossRef](#)]
109. Focke, P.; Olson, R.E.; Cariatore, N.D.; Alessi, M.; Otranto, S. Role of the recoil ion in single-electron capture and single-ionization processes for collisions of protons with He and Ar atoms. *Phys. Rev. A* **2017**, *95*, 052707. [[CrossRef](#)]
110. Olson, R.E.; Pascale, J.; Hoekstra, R. Line emission for C⁶⁺, O⁸⁺ +Li electron capture collisions. *J. Phys. B At. Mol. Opt. Phys.* **1992**, *25*, 4241–4247. [[CrossRef](#)]
111. Schippers, S.; Boduch, P.; van Buchem, J.; Blik, F.W.; Hoekstra, R.; Morgenstern, R.; Olson, R.E. Polarized light emission in keV He²⁺ + Na(3s) collisions. *J. Phys. B At. Mol. Opt. Phys.* **1995**, *28*, 3271–3282. [[CrossRef](#)]
112. Schlattmann, A.R.; Hoekstra, R.; Morgenstern, R.; Olson, R.E.; Pascale, J. Strong velocity dependence in electron capture collisions between aligned Na*(3p) and He²⁺. *Phys. Rev.-Lett.* **1993**, *71*, 513–516. [[CrossRef](#)]

113. Schippers, S.; Hoekstra, R.; Morgenstern, R.; Olson, R.E. Anisotropy and polarization in charge changing collisions of C^{4+} with $Na(3s)$ and laser aligned $Na(3p)$. *J. Phys. B At. Mol. Opt. Phys.* **1996**, *29*, 2819–2836. [[CrossRef](#)]
114. Blank, I.; Otranto, S.; Meinema, C.; Olson, R.E.; Hoekstra, R. State-selective electron transfer and ionization in collisions of highly charged ions with ground-state $Na(3s)$ and laser-excited $Na^*(3p)$. *Phys. Rev. A* **2012**, *85*, 022712. [[CrossRef](#)]
115. Otranto, S.; Blank, I.; Olson, R.E.; Hoekstra, R. Evidence of electron saddle swap oscillations in angular differential ion–atom charge exchange cross sections. *J. Phys. B At. Mol. Opt. Phys.* **2012**, *45*, 175201. [[CrossRef](#)]
116. Blank, I.; Otranto, S.; Meinema, C.; Olson, R.E.; Hoekstra, R. Angular differential studies of electron transfer in collisions of He-like ions with $Na(3s)$: The role of electron saddle crossings. *Phys. Rev. A* **2013**, *87*, 032712. [[CrossRef](#)]
117. Otranto, S.; Hoekstra, R.; Olson, R.E. Role of electron saddle swaps in the photon spectra following Li^{3+} charge-exchange collisions with $H^*(n = 2)$, $Na(3s)$, $Na^*(3p)$, and $Li(2s)$ targets. *Phys. Rev. A* **2014**, *89*, 022705. [[CrossRef](#)]
118. Otranto, S.; Olson, R.E.; Beiersdorfer, P. X-ray emission cross sections following charge exchange by multiply charged ions of astrophysical interest. *Phys. Rev. A* **2006**, *73*, 022723. [[CrossRef](#)]
119. Otranto, S.; Olson, R.E.; Beiersdorfer, P. Cometary X-rays: Line emission cross sections for multiply charged solar wind ion charge exchange. *J. Phys. B At. Mol. Opt. Phys.* **2007**, *40*, 1755–1766. [[CrossRef](#)]
120. Borbély, S.; Tökési, K.; Nagy, L. Ionization of the water by intense ultrashort half-cycle electric pulses. *Eur. Phys. J. D* **2010**, *59*, 337–348. [[CrossRef](#)]
121. Kirschbaum, C.L.; Wilets, L. Classical many-body model for atomic collisions incorporating the Heisenberg and Pauli principles. *Phys. Rev. A* **1980**, *21*, 834–841. [[CrossRef](#)]
122. Zajfman, D.; Maor, D. “Heisenberg Core” in Classical-Trajectory Monte Carlo Calculations of Ionization and Charge Exchange. *Phys. Rev. Lett.* **1986**, *56*, 320–323. [[CrossRef](#)]
123. Cohen, J.S. Quasiclassical-trajectory Monte Carlo methods for collisions with two-electron atoms. *Phys. Rev. A* **1996**, *54*, 573–586. [[CrossRef](#)] [[PubMed](#)]
124. Morita, S.; Matsuda, N.; Toshima, N.; Hino, K. Ionization of stabilized helium atoms by proton and antiproton impacts. *Phys. Rev. A* **2002**, *66*, 042719. [[CrossRef](#)]
125. Zhou, Y.U.; Huang, C.; Liao, Q.; Lu, P. Classical simulations including electron correlations for sequential double ionization. *Phys. Rev. Lett.* **2012**, *109*, 053004. [[CrossRef](#)] [[PubMed](#)]
126. Bachi, N.; Otranto, S. A closer insight into classical models for the He atom with two-active electrons. *Eur. Phys. J. D* **2018**, *72*, 127. [[CrossRef](#)]
127. Bachi, N.; Otranto, S. Evaluation of differential cross sections using classical two-active electron models for He. *Eur. Phys. J. D* **2019**, *73*, 4. [[CrossRef](#)]
128. Ziaeeian, I.; Tökési, K. State selective classical electron capture cross sections in $Be^{4+} + H(1s)$ collisions with mimicking quantum effect. *Sci. Rep.* **2021**, *11*, 20164. [[CrossRef](#)]
129. Ziaeeian, I.; Tökési, K. The effects of Heisenberg constraint on the classical cross sections in proton hydrogen collision. *J. Phys. B At. Mol. Opt. Phys.* **2022**, *55*, 245201. [[CrossRef](#)]
130. Pfeiffer, S.J.; Olson, R.E. Electron removal from helium by fast, multiply charged ions. *Phys. Lett.* **1982**, *92A*, 175–178. [[CrossRef](#)]
131. Olson, R.E. Collisional mechanisms for single and double ionization of He by protons and antiprotons. *Phys. Rev. A* **1986**, *33*, 1519–1521. [[CrossRef](#)]
132. McKenzie, M.L.; Olson, R.E. Ionization and charge exchange in multiply-charged-ion-helium collisions at intermediate energies. *Phys. Rev. A* **1987**, *35*, 2863–2868. [[CrossRef](#)]
133. Olson, R.E.; Wetmore, A.E.; McKenzie, M.L. Double electron transitions in collisions between multiply charged ions and helium atoms. *J. Phys. B At. Mol. Phys.* **1986**, *19*, L629–L634. [[CrossRef](#)]
134. Tökési, K.; Hock, G. Double electron capture in $He^{2+} + He$ collisions up to 1500 keV/amu projectile impact. *J. Phys. B At. Mol. Phys.* **1996**, *29*, L119–L125. [[CrossRef](#)]
135. Montemayor, V.J.; Schiwietz, G. Dynamic target screening for two-active-electron classical-trajectory Monte Carlo calculations for $H^+ + He$ collisions. *Phys. Rev. A* **1989**, *40*, 6223–6230. [[CrossRef](#)] [[PubMed](#)]
136. Meng, L.; Olson, R.E.; Dörner, R.; Ullrich, J.; Schimdt-Böcking, H. Differential cross sections for single and double ionization of helium by protons and antiprotons. *J. Phys. B At. Mol. Opt. Phys.* **1993**, *26*, 3387–3401. [[CrossRef](#)]
137. Mergel, V.; Dörner, R.; Ullrich, J.; Jagutzki, O.; Lencinas, S.; Nüttgens, S.; Spielberger, L.; Unverzagt, M.; Cocke, C.L.; Olson, R.E.; et al. State Selective Scattering Angle Dependent Capture Cross Sections Measured by Cold Target Recoil Ion Momentum Spectroscopy. *Phys. Rev. Lett.* **1995**, *74*, 2200–2203. [[CrossRef](#)]
138. Alessi, M.; Otranto, S.; Focke, P. State-selective electron capture in $^3He^{2+} + He$ collisions at intermediate impact energies. *Phys. Rev. A* **2011**, *83*, 014701. [[CrossRef](#)]
139. Peters, M.B.; Katsoulis, G.P.; Emmanouilidou, A. General model and toolkit for the ionization of three or more electrons in strongly driven atoms using an effective Coulomb potential for the interaction between bound electrons. *Phys. Rev. A* **2022**, *105*, 043102. [[CrossRef](#)]
140. Bonham, R.A.; Kohl, D.A. Simple correlated wavefunctions for the ground state of heliumlike atoms. *J. Chem. Phys.* **1966**, *45*, 2471–2473. [[CrossRef](#)]
141. Geyer, T.; Rost, J.M. A quasi-classical approach to fully differential ionization cross sections. *J. Phys. B At. Mol. Phys.* **2001**, *34*, L47–L53. [[CrossRef](#)]

142. Geyer, T.; Rost, J.M. A quasi-classical approach to electron impact ionization. *J. Phys. B At. Mol. Phys.* **2001**, *35*, 1479–1499. [[CrossRef](#)]
143. Geyer, T.; Rost, J.M. Dynamical stabilization of classical multi-electron targets against autoionization. *J. Phys. B At. Mol. Phys.* **2001**, *36*, L107–L112. [[CrossRef](#)]
144. Geyer, T. Electron impact double ionization of helium from classical trajectory calculations. *J. Phys. B At. Mol. Phys.* **2004**, *37*, 1215–1235. [[CrossRef](#)]
145. Haan, S.L.; Breen, L.; Karim, A.; Eberly, J.H. Variable time lag and backward ejection in full-dimensional analysis of strong-field double ionization. *Phys. Rev. Lett.* **2006**, *97*, 103008. [[CrossRef](#)] [[PubMed](#)]
146. Haan, S.L.; Breen, L.; Karim, A.; Eberly, J.H. Recollision dynamics and time delay in strong-field double ionization. *Opt. Expr.* **2007**, *15*, 767–778. [[CrossRef](#)] [[PubMed](#)]
147. Su, Q.; Eberly, J.H. Model atom for multiphoton physics. *Phys. Rev. A* **1991**, *44*, 5997–6008. [[CrossRef](#)]
148. Panfili, R.; Haan, S.L.; Eberly, J.H. Comparing classical and quantum dynamics of strong-field double ionization. *Opt. Expr.* **2001**, *8*, 431–435. [[CrossRef](#)]
149. Panfili, R.; Haan, S.L.; Eberly, J.H. Slow-down collisions and nonsequential double ionization in classical simulations. *Phys. Rev. Lett.* **2002**, *89*, 113001. [[CrossRef](#)]
150. Sarkadi, L. Laser-induced nonsequential double ionization of helium: Classical model calculations. *J. Phys. B At. Mol. Opt. Phys.* **2020**, *53*, 165401. [[CrossRef](#)]
151. Huang, C.; Zhou, Y.; Zhang, Q.; Lu, P. Contribution of recollision ionization to the cross-shaped structure in nonsequential double ionization. *Opt. Expr.* **2013**, *21*, 11382–11390. [[CrossRef](#)]
152. Ma, X.; Li, M.; Zhou, Y.; Lu, P. Nonsequential double ionization of Xe by mid-infrared laser pulses. *Opt. Expr.* **2013**, *21*, 11382–11390. [[CrossRef](#)]
153. Guzmán, F.; Errea, L.F.; Pons, B. Two-active electron classical trajectory Monte Carlo methods for ion-He collisions. *Phys. Rev. A* **2009**, *80*, 042708. [[CrossRef](#)]
154. Olson, R.E.; Ullrich, J.; Schmidt-Böcking, H. Dynamics of multiply charged ion-atom collisions: $U^{32+} + Ne$. *J. Phys. B At. Mol. Phys.* **1987**, *20*, L809–L814. [[CrossRef](#)]
155. Olson, R.E.; Ullrich, J.; Schmidt-Böcking, H. Multiple-ionization collision dynamics. *Phys. Rev. A* **1989**, *39*, 5572–5583. [[CrossRef](#)]
156. Tókési, K. Double electron excitation of helium by charged particle impact. *Nucl. Instr. Methods Phys. Res. B* **2005**, *233*, 266–269. [[CrossRef](#)]
157. Borbély, S.; Feist, J.; Tókési, K.; Nagele, S.; Nagy, L.; Burdörfer, J. Ionization of helium by slow antiproton impact: Total and differential cross sections. *Phys. Rev. A* **2014**, *90*, 052706. [[CrossRef](#)]
158. Tókési, K.; Paripás, B.; Kovács, E. Classical trajectory Monte Carlo simulation of coincidence experiments in electron impact ionization of helium. *Eur. Phys. J. D* **2019**, *73*, 84. [[CrossRef](#)]
159. Otranto, S.; Olson, R.E. X-ray emission cross sections following Ar^{18+} charge-exchange collisions on neutral argon: The role of the multiple electron capture. *Phys. Rev. A* **2011**, *83*, 032710. [[CrossRef](#)]
160. Giese, J.P.; Horsdal, E. Structure in the differential charge-state fractions of the following ionization by fast protons. *Phys. Rev. Lett.* **1988**, *60*, 2018–2021. [[CrossRef](#)]
161. Olson, R.E.; Ullrich, J.; Dörner, R.; Schmidt-Böcking, H. Single- and double-ionization cross sections for angular scattering of fast protons by helium. *Phys. Rev. A* **1989**, *40*, 2843–2846. [[CrossRef](#)]
162. Dörner, R.; Ullrich, J.; Olson, R.E.; Jagutzki, O.; Schmidt-Böcking, H. Azimuthal angular dependence of recoil-ion and electron emission in 0.5 MeV p + He collisions. *Phys. Rev. A* **1993**, *47*, 3845–3851. [[CrossRef](#)]
163. Meng, L.; Reinhold, C.O.; Olson, R.E. Electron removal from molecular hydrogen by fully stripped ions at intermediate energies. *Phys. Rev. A* **1989**, *40*, 3637–3645. [[CrossRef](#)] [[PubMed](#)]
164. Meng, L.; Olson, R.E.; Folkerts, H.O.; Hoekstra, R. State-selective electron capture in He^{2+} - H_2 collisions. *J. Phys. B At. Mol. Opt. Phys.* **1994**, *27*, 2269–2276. [[CrossRef](#)]
165. Wood, C.J.; Olson, R.E. Double electron removal and fragmentation model of the H_2 molecule by highly charged ions. *Phys. Rev. A* **1999**, *59*, 1317–1328. [[CrossRef](#)]
166. Alessi, M.; Cariatore, N.D.; Focke, P.; Otranto, S. State-selective electron capture in $He^+ + H_2$ collisions at intermediate impact energies. *Phys. Rev. A* **2012**, *85*, 042704. [[CrossRef](#)]
167. Greenspan, D. Electron attraction as a mechanism for the chemical bond of ground state H_2^* . *Phys. Scr.* **1995**, *52*, 267–270. [[CrossRef](#)]
168. Greenspan, D. Dynamical generation of electron motions in ground state H_2^+ , in ground state H_2 and in the first excited state of H_2 . *Phys. Scr.* **1995**, *55*, 277–285. [[CrossRef](#)]
169. Hennecart, D.; Pascale, J. Classical approach to $H_2^+ - H(1s)$ collisions. *Phys. Rev. A* **2005**, *71*, 012710. [[CrossRef](#)]
170. Jorge, A.; Horbatsch, M.; Illescas, C.; Kirchner, T. Classical-trajectory Monte Carlo calculations of differential electron-emission cross sections in fast heavy-ion collisions with water molecules. *Phys. Rev. A* **2019**, *99*, 062701. [[CrossRef](#)]
171. Jorge, A.; Horbatsch, M.; Kirchner, T. Multicharged-ion-water-molecule collisions in a classical-trajectory time-dependent mean-field theory. *Phys. Rev. A* **2020**, *102*, 012808. [[CrossRef](#)]
172. Sarkadi, L. Classical treatment of the electron emission from collisions of uracil molecules with fast protons. *Phys. Rev. A* **2015**, *92*, 062704. [[CrossRef](#)]

173. Sarkadi, L. Classical trajectory Monte Carlo model calculations for ionization of the uracil molecule by impact of heavy ions. *J. Phys. B At. Mol. Opt. Phys.* **2016**, *49*, 185203. [[CrossRef](#)]
174. Cariatore, N.D.; Otranto, S. Development and evaluation of a many-electron-multicenter classical-trajectory Monte Carlo model in charge-exchange processes involving collisions of multiple charged ions and CO. *Phys. Rev. A* **2013**, *88*, 012714. [[CrossRef](#)]
175. Abbas, I.; Champion, C.; Lasri, B.; Hanssen, J. Single and multiple cross sections for ionizing processes of biological molecules by protons and α -particle impact: A classical Monte Carlo approach. *Phys. Med. Biol.* **2008**, *53*, N41–N51. [[CrossRef](#)]
176. Lekadir, H.; Abbas, I.; Champion, C.; Fojón, O.; Rivarola, R.D.; Hanssen, J. Single-electron-loss cross sections of DNA and RNA bases impacted by energetic multicharged ions: A classical Monte Carlo approximation. *Phys. Rev. A* **2009**, *79*, 062710. [[CrossRef](#)]
177. Lekadir, H.; Abbas, I.; Champion, C.; Hanssen, J. Total cross sections for ionizing processes induced by proton impact on molecules of biological interest: A classical trajectory Monte Carlo approach. *Nucl. Instr. Meth. B* **2009**, *267*, 1011–1014. [[CrossRef](#)]
178. Bachi, N.; Otranto, S.; Otero, G.S.; Olson, R.E. The role of multiple ionization of H₂O in heavy ion collisions. *Phys. Med. Biol.* **2019**, *64*, 205020. [[CrossRef](#)]
179. Bhattacharjee, S.; Biswas, S.; Monti, J.M.; Rivarola, R.D.; Tribedi, L.C. Double differential cross section for ionization of H₂O molecules by 4 MeV/u C⁶⁺ and Si¹³⁺ ions. *Phys. Rev. A* **2017**, *96*, 052707. [[CrossRef](#)]
180. Bhattacharjee, S.; Bagdia, C.; Roy Chowdhury, M.; Monti, J.M.; Rivarola, R.D.; Tribedi, L.C. Energy and angular distributions of electrons ejected from water by the impact of O⁸⁺ ion beams. *Eur. Phys. J. D* **2018**, *72*, 15. [[CrossRef](#)]
181. Cariatore, N.D.; Bachi, N.; Otranto, S. C⁶⁺ impact ionization of uracil at MeV/u impact energies: The role of the multiple ionization channel. *Phys. Rev. A* **2022**, *106*, 012808. [[CrossRef](#)]
182. Ralchenko, Y.; Maron, Y. Accelerated recombination due to resonant deexcitation of metastable states. *J. Quant. Spectr. Rad. Transf.* **2001**, *71*, 609–621. [[CrossRef](#)]
183. Machacek, J.R.; Mahapatra, D.P.; Schultz, D.R.; Ralchenko, Y.; Chutjian, A.; Simcic, J.; Mawhorter, R.J. Measurement and calculation of absolute single- and double-charge-exchange cross sections for O⁶⁺ ions at 1.17 and 2.33 keV/u impacting He and H₂. *Phys. Rev. A* **2014**, *90*, 052708. [[CrossRef](#)]
184. Machacek, J.R.; Mahapatra, D.P.; Schultz, D.R.; Ralchenko, Y.; Moradmand, A.; El Ghazaly, M.O.A.; Chutjian, A. Solar-wind ion-driven x-ray emission from cometary and planetary atmospheres: Measurements and theoretical predictions of charge-exchange cross-sections and emission spectra for O⁶⁺ + H₂O, CO, CO₂, CH₄, N₂, NO, N₂O, and Ar. *Astr. J.* **2015**, *809*, 75. [[CrossRef](#)]
185. Ali, R.; Cocke, C.L.; Raphaelian, M.L.A.; Stockli, M. Multielectron processes in 10-keV/u Ar^{q+} (5 ≤ q ≤ 17) on Ar collisions. *Phys. Rev. A* **1994**, *49*, 3586–3596. [[CrossRef](#)] [[PubMed](#)]
186. Salehzadeh, A.; Kirchner, T. Strong multiple-capture effect in slow Ar¹⁷⁺-Ar collisions: A quantum mechanical analysis. *J. Phys. B At. Mol. Opt. Phys.* **2013**, *46*, 025201. [[CrossRef](#)]
187. Otranto, S.; Cariatore, N.D.; Olson, R.E. X-ray emission produced in charge-exchange collisions between highly charged ions and argon: Role of the multiple electron capture. *Phys. Rev. A* **2014**, *90*, 062708. [[CrossRef](#)]
188. Cariatore, N.D. Modelado de Blancos Atómicos y Moleculares en Física de Colisiones por Impacto de Iones en CTMC. Ph.D. Thesis, Universidad Nacional del Sur, Bahía Blanca, Argentina, 2015.
189. Tawara, H.; Takács, E.; Suta, T.; Makónyi, K.; Ratliff, L.P.; Gillaspay, J.D. K x rays produced in collisions of bare ions with atoms: Contribution of multiple-electron transfer in, Kr³⁶⁺, Ar¹⁸⁺, and Ne¹⁰⁺ + Ar collisions. *Phys. Rev. A* **2006**, *73*, 012704. [[CrossRef](#)]
190. Allen, F.I.; Biedermann, C.; Radtke, R.; Fussmann, G.; Fritzsche, S. Energy dependence of angular momentum capture states in charge exchange collisions between slow highly charged argon ions and argon neutrals. *Phys. Rev. A* **2008**, *78*, 032705. [[CrossRef](#)]

Disclaimer/Publisher's Note: The statements, opinions and data contained in all publications are solely those of the individual author(s) and contributor(s) and not of MDPI and/or the editor(s). MDPI and/or the editor(s) disclaim responsibility for any injury to people or property resulting from any ideas, methods, instructions or products referred to in the content.